

NATIONAL INSTITUTE FOR FUSION SCIENCE

Recommended Data on Electron-ion Collision Strengths and
Effective Collision Strengths for Fe X, Fe XI and Fe XIII Ions

I. Skobelev, I. Murakami and T. Kato

(Received - Jan. 21, 2009)

NIFS-DATA-104

Jan. 29, 2009

RESEARCH REPORT
NIFS-DATA Series

TOKI, JAPAN

This report was prepared as a preprint of work performed as a collaboration research of the National Institute for Fusion Science (NIFS) of Japan. The views presented here are solely those of the authors. This document is intended for information only and may be published in a journal after some rearrangement of its contents in the future.

Inquiries about copyright should be addressed to the Research Information Office, National Institute for Fusion Science, Oroshi-cho, Toki-shi, Gifu-ken 509-5292 Japan.

E-mail: bunken@nifs.ac.jp

<Notice about photocopying>

In order to photocopy any work from this publication, you or your organization must obtain permission from the following organization which has been delegated for copyright for clearance by the copyright owner of this publication.

Except in the USA

Japan Academic Association for Copyright Clearance (JAACC)
6-41 Akasaka 9-chome, Minato-ku, Tokyo 107-0052 Japan
Phone: 81-3-3475-5618 FAX: 81-3-3475-5619 E-mail: jaacc@mtd.biglobe.ne.jp

In the USA

Copyright Clearance Center, Inc.
222 Rosewood Drive, Danvers, MA 01923 USA
Phone: 1-978-750-8400 FAX: 1-978-646-8600

**RECOMMENDED DATA ON ELECTRON-ION COLLISION STRENGTHS
AND EFFECTIVE COLLISION STRENGTHS FOR FE X, FE XI, and FE XIII
IONS.**

Skobelev, I.⁽¹⁾⁽²⁾⁽³⁾, Murakami, I.⁽¹⁾, Kato, T.⁽¹⁾

⁽¹⁾ National Institute for Fusion Science, Oroshi-cho, Toki, Gifu, 509-5292, Japan

*⁽²⁾ Multicharged Ions Spectra Data Center of VNIIFTRI, Mendeleevo, Moscow region,
141570 Russia*

*⁽³⁾ Associated Institute for High Temperatures Russian Academy of Sciences, Izhorskaya
13/19, Moscow, 125412 Russia*

Abstract.

Data obtained for electron-induced excitation transitions between levels with principal quantum numbers $n=3$ in Cl-like Fe X, S-like Fe XI, and Si-like Fe XIII ions by different theoretical methods were compared, and recommended data for electron collision strengths and effective collision strengths have been chosen. Simple analytical formulas with 7 free parameters were used to describe electron temperature dependence of effective collision strengths in a wide temperature range. The values of free parameters have been determined by fitting the recommended numerical data. The obtained results can be used for plasma kinetics calculations and for spectroscopic methods of plasma diagnostics.

Keywords: electron-ion collisions, excitation, plasma spectroscopy, ion kinetics.

1. Introduction

Iron is an abundant element in both laboratory and astrophysical plasmas, and its spectral lines have been observed for all ionization stages. The Fe IX - Fe XVI ions have strong resonance transitions in the extreme ultraviolet spectral range $\sim 170 - 400 \text{ \AA}$. These ions are formed, for example, in the solar corona, and the resonance transitions are prominent in solar spectra. In addition, some forbidden transitions of these ions appear in the ultraviolet region in solar spectra. All these transitions are expected to be present in the spectra of magnetically confined plasma, as well as in the spectra of different astrophysical objects such as solar coronae or late-type stars.

In order to interpret the observable data and to develop spectroscopic methods of plasma diagnostics it is necessary to have accurate atomic data concerning these ions, such as data on collision strengths Ω and effective collision strengths Γ for electron impact excitation. There are few experimental measurements for electron impact excitation cross sections (collision strengths) and so reliable theoretical atomic data are required for the purpose of diagnostics and plasma modeling.

In this paper we discuss collision data for Cl-like Fe (Fe X), S-like Fe (Fe XI), and Si-like Fe (Fe XIII) ions. Note, that the number of collision transitions even among configurations with principal quantum number $n = 3$ is very high and it is practically impossible to compare different collision data for all possible transitions. Therefore we will base our analysis mainly on comparison of effective collision strengths for ion levels which are responsible for emission of the most intense spectral lines in the far-ultraviolet spectral band 200-300 \AA .

At present time there are many papers giving calculations of effective electron collision strengths Γ_{ij} for different Fe ions. In these papers the effective electron collision strengths were published in tabular form. For many applications this form of data presentation is not convenient, and some analytical formula $\Gamma_{ij}(T_e)$ would be preferable. Therefore, the purpose of the present work was not only evaluation of electron excitation rates calculated for Fe X, XI, XIII ions with the help of different methods, but also choice of simple functions allowing us to describe dependencies $\Gamma_{ij}(T_e)$ for all transitions considered.

2. Calculation methods and comparisons.

2.1 Excitation of $n=3 - n'=3$ transitions in Fe X by electron impact.

In the past 10 years a variety of calculations have performed to compute various atomic parameters of this ion. The most notable among the available calculations, particularly for collision strengths Ω and effective collision strengths Γ , are calculations carried out by Bhatia & Doschek [1], Tayal [2], Pelan & Berrington [3] and Aggarwal [4].

In paper [1] results for energy levels, radiative rates and collision strengths for all transitions among 54 levels of the $3s^23p^5$, $3s3p^6$, $3s^23p^43d$ and $3s3p^53d$ configurations were presented. In this work the Superstructure (SS) code of Eissner et al [5] was used for the generation of wavefunctions, and the Distorted-Wave (DW) code of Eissner & Seaton [6] was used for the computation of Ω . These calculations are basically in LS coupling, and results for transitions in intermediate coupling (LSJ) were obtained through an algebraic transformation using the *JAJOM* program of Saraph [7]. One-body relativistic effects were included in the calculations through term coupling coefficients. However, these calculations are limited for two reasons. First, their wave functions are not highly accurate, because many of their energy levels differ with experimental and other theoretical results by $\sim 4-7\%$ (see Table 1). This has a direct effect on the subsequent calculations of radiative rates and collision strengths, which may easily vary by a factor of ~ 2 for strong transitions, and by larger factors for weaker transitions [2]. The main reason for this inaccuracy is the neglect of configuration interaction (CI) with additional configurations, as CI is very important for Fe X. Second, in [1] the values of Ω are presented at only 5 energies above thresholds, and resonances in the thresholds region are not taken into account. Therefore, results obtained for Γ from such a limited set of Ω 's can be underestimated by up to an order of magnitude, especially for the forbidden transitions.

In papers [2] Tayal attempted to remove both the limitations of the calculations [1]. For the generation of wave functions additional configurations were included (mainly with the $4l$ orbitals), and resonances were resolved in order to improve the accuracy of the Γ results. In this work CIV3 program of Hibbert [8] was applied for the generation of wave functions, and the R-matrix code of Berrington et al [9] was used for the computation of Ω . These calculations were performed in LSJ coupling, and one-body relativistic effects were included through the Breit-Pauli approximation. However, these

calculations are also limited for two main reasons. First, energies calculated for the lowest 24 levels are the highest among all the available theoretical results, and are higher by up to 8% in comparison with the experimental ones. Additionally, the orderings of energy levels agree neither with the experimental ones nor with any of the CI calculations. Second, in these calculations 10 metastable levels were excluded. The omission of these levels affects the resonance pattern in the threshold region, and subsequently affects their contributions in the determination of Γ values.

An approach analogous to [2] was used in paper [3]. In this work calculations have performed also in *LSJ* coupling through the Breit-Pauli approximation, and the CIV3 and R-matrix programs were employed for the generation of wave functions and computations of Γ , respectively. Extensive configuration interaction have been included in the generation of wave functions, which is clearly reflected by the excellent agreement of their energy levels with both experimental ones and other theoretical results. Additionally, in this work resonances have been resolved on a fine energy mesh, and hence results [3] for all atomic parameters should be comparatively more accurate than [1, 2]. However, first, the results are limited to transitions from the lowest three levels to higher excited levels, and, second, there is still some concern about the accuracy of the results.

The results [3] for Γ differ from those of [2] by a factor of two for many transitions. These substantial differences are not confined to any particular range of temperature. Similarly values of Ω obtained in [3] differ from [2] by a factor of two for some of the allowed transitions, in spite of the fact that the transition energies and oscillator strengths are comparable in both calculations. Since both of these calculations are contemporary, of comparable accuracy, and use the same methodology (the R-matrix code in the Breit-Pauli approximation), such large differences for many important transitions are not expected. Therefore, in order to assess the accuracy of the available data for Ω and Γ , as well as to extend the range of transitions, calculations based on an independent approach were carried out in paper [4]. Contrary to the [2, 3] approach, the calculations of [4] are fully relativistic and are based on GRASP code of Dyall et al [10] for the generation of wave functions, and the Dirac Atomic R-matrix Code (DARC) of Norrington et al [11] for the computations of collision and effective collision strengths.

In reference [4] the authors considered the lowest 90 levels of the $3s^23p^5$, $3s3p^6$, $3s^23p^43d$, $3s3p^53d$ and $3s^23p^33d^2$ configurations of Fe X ion. To generate the wave functions, they used the fully relativistic GRASP code with the option of extended average level, in which a weighted (proportional to $2j + 1$) trace of the Hamiltonian matrix was minimized. This produced a compromise set of orbitals describing closely lying states with moderate accuracy. Their calculations were in the jj coupling scheme, and the Breit and QED corrections were included. The CI was included among the configurations $3s^23p^5$, $3s3p^6$, $3s^23p^43d$, $3s3p^53d$, $3s^23p^33d^2$, $3p^63d$, $3s3p^43d^2$, $3s^23p^23d^3$, and some energy levels obtained are shown in Table 1. It is seen that the accuracy of energy levels [4] is better than 3%. For the computations of collision strengths the DARC program was employed. This program includes the relativistic effects in a systematic way, in both the target description and the scattering model. It is based on the jj coupling scheme, and uses the Dirac-Coulomb Hamiltonian in the R-matrix approach. However, because of the inclusion of fine-structure in the definition of channel coupling, the matrix size of the Hamiltonian increases substantially, making the calculations computationally expensive. The R-matrix radius was adopted to be 3.28 au, and 21 continuum orbitals were included for each channel angular momentum for the expansion of the wave function. This allowed computation of Ω up to an energy of 210 Ryd. The maximum number of channels for a given partial wave was 538, and the corresponding size of the Hamiltonian matrix was 11340×11340 . In order to obtain convergence of Ω for all transitions and at all energies all partial waves with angular momentum $J < 39$ were included. In Figure 1, the variation of Ω is shown with angular momentum J at three energies of 10, 50 and 200 Ryd, and for 2 transitions, 1-3 ($3s^23p^5 \ ^2P_{3/2}$ - $3s3p^6 \ ^2S_{1/2}$) and 3-26 ($3s3p^6 \ ^2S_{1/2}$ - $3s^23p^4(^1S)3d \ ^2D_{5/2}$), which are allowed and forbidden transitions, respectively. For the forbidden transitions, such as 3-26 shown in Fig. 1a, the calculations of Ω are practically fully converged at all energies, including the highest energy 210 Ryd. For allowed transitions, such as 1-3 shown in Fig. 1b, Ω are converged within range of partial waves $J < 39$ only at energies below 50 Ryd. It is clearly seen from Fig. 1, that calculations limited by smaller values of J will not give correct results. In particular, the limitation $J < 11$ by Mohan et al [12] decreases accuracy of data very strongly.

In Figures 2 and 3 we present dependencies $\Omega(E)$ for transitions from the ground state $3s^23p^5 \ ^2P_{3/2}$ to excited levels $3s3p^6 \ ^2S_{1/2}$ and $3s^23p^4(^3P)3d \ ^4D_{5/2}$ calculated in [1-4].

These results are useful in assessing the accuracy of a calculation. Since wave functions used in [1] are different from wave functions used in [4], disagreements in the values of Ω from [1] and [4] are not unexpected. However, for most of the allowed transitions, the differences in these two sets of Ω are in accordance with their corresponding f-values, and this is clearly seen from Fig. 4. It is more surprising that results of [3] for forbidden transitions are in agreement with all other calculations and for the allowed transitions disagree strongly with the other works. In spite of the f-values for the 1-3 and 2-3 transitions, for example, being comparable with those of [2, 4], the values of Ω from [3] are lower by a factor of two, and are not in accordance with the expected behavior. Since the Ω -values of [3] are nearly constant for the 1-3 and 2-3 allowed transitions in the entire energy range of 18-45 Ryd, one has an impression that for at least these energies, the results are not converged. Since the authors of [3] have included all partial waves with angular momentum $J < 56$, the results for Ω should be converged, as is apparent from Fig. 1b for the 1-3 transition. Analysis carried out in [4] allow one to conjecture that calculations in [3] might have included all partial waves with $J < 56$ for energies towards the higher end of their calculations of Ω , but perhaps a limited range of partial waves for the calculations at energies below ~ 50 Ryd ($J < 8$, $J < 10$ and $J < 12$ for calculation at $E = 18, 27$ and 45 Ryd, correspondingly). Thus we conclude that for allowed transitions, and at least at energies below ~ 50 Ryd, the Ω values of [3] are not converged, due to the inclusion of a limited range of partial waves. Since this energy region is very important for calculations of Γ at temperatures below 7×10^6 K, the results [3] for the effective collision strengths are expected to be underestimated, especially for the allowed transitions. Some of the forbidden transitions will also be affected but not to the same extent as the allowed transitions.

Thus we see that at present time the most accurate values of Ω for Cl-like Fe (Fe X) ion have been probably obtained in work [4]. Authors of this work estimate the accuracy of their collision strengths as 10% (and as 20% for effective collision strengths) or even better, at all energies and for all transitions considered.

Figures 5-11 present the dependencies of effective collision strengths Γ on plasma electron temperature T_e for 11 transitions causing emission of the most intense Fe X spectral lines in the spectral region 170 -290 Å. These dependencies were calculated in papers [2-4, 12].

The most interesting points among them are that data calculated in [2-4] cause strong decrease of the accuracy of data obtained in paper [12], because of limitation for partial waves $J < 11$, as it was noted above, as well as the inaccurate wave functions.

Although all three sets of calculations [2-4] are based on the R-matrix method, including CI and relativistic effects in the generation of wave functions, and all three have resolved resonances in threshold region, the values of Γ show poor agreement for a majority of transitions. Different sets of results differ by up to a factor of two. However, such large differences among different calculations are fully understandable.

First of all, it is necessary to emphasize the specific differences between calculations [4] and [2, 3]. First, calculations [4] are fully relativistic and in jj coupling, which not only properly accounts for the relativistic effects, but also shows comparatively more resonances because of the inclusion of fine-structure in the definition of channel coupling. In contrast, the calculations [2, 3] are semi-relativistic in the LSJ coupling scheme, and do not account for the two-body relativistic operators. Second, the wave functions used in [4] include larger CI than those of [2] or [3], which improves the accuracy of the energy levels and radiative rates, and subsequently of Ω and Γ . Third, calculations in [4] include a larger range of partial waves ($J < 39$) than those of [2] ($J < 20$) or of [3] (see above). This improves the accuracy of the Ω values, not only for the allowed transitions but for the forbidden ones also. Similarly, calculations [4] cover a wider range of energy, i.e. $E < 210$ Ryd in comparison to $E < 90$ Ryd of [2]. Finally, calculations [4] include 90 levels, whereas those of [2] and [3] include 54 and 31 levels, respectively.

Fe X is one of the rare ions for which some experimental results are available for comparison for many atomic parameters, namely energy levels, life-times, cross sections and excitation rates. Wang & Griem [13] have measured statistically averaged excitation rates from the ground state $3s^23p^5\ ^2P$ to higher excited levels of the $3p^43d$ configuration, at three electron temperatures of 45, 75 and 95 eV. Their results are compared in Figures 12-16 with corresponding theoretical rates calculated in [2, 3, 4]. It can be seen from these figures that experimental accuracy ~ 30 -60% is not enough good to estimate the accuracy of theoretical calculations. Probably the experimental results [13] are overestimated for almost all transitions and at all temperatures. Taking experimental accuracy into

consideration, we may state that theory and experiment are in satisfactory agreement especially at high temperatures.

The results presented in paper [4] have obvious advantages in comparison with the earlier results of [1-3]. In comparison with the work [1], calculations [4] have significantly improved the accuracy of energy levels, radiative rates and collision strengths, by including extensive CI and performing the calculations in the *jj* coupling. In comparison to the work [2] an overall improvement has been made by: (i) including additional CI in the generation of wave functions, and thus improving the accuracy of energy levels; (ii) extending the range of levels from 54 to 90, and hence including many of the desired levels among which the transitions have already been observed; (iii) improving the accuracy of Ω values, by extending the range of partial waves (from 20 to 39) and the energy range (from 90 Ryd to 210 Ryd); (iv) improving the Γ values by resolving resonances in a finer energy mesh and by including additional resonances; (v) performing the calculations in the *jj* coupling instead of the semi-relativistic approach in the *LSJ* coupling scheme. Similarly, the work [4] is an improvement over the work [3] mainly by extending the range of levels (transitions) from 31 (465) to 90 (4005), and by achieving convergence in values of Ω at all energies.

It should be noted that in the CHIANTI atomic database less accurate data [3] are used for transitions between $3s^23p^5$, $3s3p^6$ and $3s^23p^43d$ configurations (31 levels), distorted wave approximation is used for transitions to $3s3p^53d$ configuration (levels up to 54) and approximate calculations [14] are used for levels 55-172 (see, for example, Del Zanna et al [15]). We recommend to use for the first 90 levels single data set [4].

2.2 Excitation of $n=3 - n'=3$ transitions in S-like Fe XI by electron impact.

Calculations for Fe XI ion have been performed with the help of several theoretical methods.

The calculations of collision strengths in work of Bhatia & Doschek [16] were carried out in the distorted wave approximation. This approximation neglects autoionizing resonances in excitation cross sections due to dielectronic capture that are explicitly accounted for in close coupling calculations. The resonances may be not very important for strong electric dipole allowed transitions but they are very significant for weak forbidden or intercombination transitions. The energy levels and oscillator

strengths were calculated using the superstructure program described by Eissner et al [5]. The wave functions were of the configuration interaction type, where each individual configuration was an expansion in terms of Slater states built from Slater-type orbitals. The configurations $3s^23p^4$, $3s3p^5$, $3s^23p^33d$, and $3p^6$ were considered. The radial functions were calculated assuming a modified Thomas-Fermi potential. The spin-orbit interaction and relativistic corrections were treated as perturbations to the non-relativistic Hamiltonian. The differences between the calculated and experimental energies are less than about 8% for the $3p^4$ ground configuration and less than about 3% for the higher levels. The scattering problem was carried out in the distorted wave approximation using the programs described by Eissner & Seaton [6]. The reactance matrices were calculated in *LS* coupling. The collision strengths in intermediate coupling were calculated using these reactance matrices and the term-coupling coefficients obtained from structure calculations in the program JAJOM of Saraph [7]. The distorted wave calculations were carried out including intermediate angular momentum states L^T up to 21. For higher partial waves the Coulomb-Bethe approximation of Burgess & Sheorey was used [22]. The electron excitation rate coefficients were obtained by integrating the collision strengths over a Maxwellian electron velocity distribution. The electron excitation rates are calculated by fitting the collision strengths at three energies with a polynomial. In paper [16] collision strengths for the 48 levels of the configurations $3s^23p^4$, $3s3p^5$, $3s^23p^33d$, and $3p^6$ are presented.

In paper of Gupta & Tayal [18] extensive semirelativistic R-matrix calculations for electron impact excitation of Fe XI ion including electron correlation, relativistic, and resonance effects were carried out. The relativistic effects were included in the Breit-Pauli approximation via the one-body mass correction, Darwin, and spin-orbit interaction terms in the scattering equations [23]. In this work, 20 LS states, $3s^23p^4$ $^3P, ^1D, ^1S$; $3s3p^5$ $^1, ^3P$; $3s^23p^3(^4S)3d$ 3D , $3s^23p^3(^2P)3d$ $^1, ^3P, ^1, ^3D, ^1, ^3F$; $3s^23p^3(^2D^o)3d$ $^1, ^3S, ^1, ^3P, ^1, ^3D, ^1, ^3F$ states of the Fe XI ion were considered and these were represented by configuration interaction wave functions. Later Gupta & Tayal [19] extended their earlier work to the transitions involving all the higher levels belonging to the $3s^23p^33d$ configuration. They used the 1s, 2s, 2p, 3s, and 3p radial functions as the Hartree-Fock functions given by Clementi & Roetti [24] for the ground $3s^23p^4$ 3P state. The radial functions 3d and 4f were chosen to give the best over all representation of the energies of

the states. The scattering wave function for each total angular momentum J and parity π combination was expanded in the inner region ($r < a$) in the R-matrix basis. They chose a boundary radius $a = 3.4$ au and included 19 continuum orbitals for each angular momentum to obtain convergence in the energy range up to 40 Ryd. The coupled equations were solved in the asymptotic region using a perturbation method to yield K-matrices and then the collision strengths. The R-matrix method was used to calculate partial collision strengths from $J = 0.5$ to $J = 17.5$. The contributions from the higher partial waves, needed for the dipole-allowed transitions, were calculated using the Bethe approximation [22]. The effective collision strengths are presented in [18, 19, 2] for all transitions among the 38 fine-structure levels.

In papers of Aggarwal & Keenan [20, 21] a fully relativistic approach was used. To calculate level energies, oscillator strengths and radiative rates for allowed transitions among $(1s^2 2s^2 2p^6) 3s^2 3p^4$, $3s 3p^5$, $3s^2 3p^3 3d$ and $3p^6$ configurations of Fe XI ion, Aggarwal & Keenan have adopted the GRASP (General purpose Relativistic Atomic Structure Program) code of Dyaall et al [10]. Thus relativistic effects were fully taken into account, unlike earlier calculations which neglected the two-body relativistic operators. Configuration interaction among the additional $3s^2 3p^2 3d^2$, $3s^2 3p^3 4s$, $3s^2 3p^3 4p$ and $3s^2 3p^3 4d$ configurations were also included. The 4f orbital was excluded from calculations in [20, 21], because its inclusion results in an additional 40 levels, but it makes a negligible difference to the values of transition energies and radiative rates. For the computations of collision strengths Ω the recently developed Dirac Atomic R-matrix Code (DARC) of Norrington et al [11] was used. This program is based on the jj coupling scheme, and uses the Dirac-Coulomb Hamiltonian in the R-matrix approach. The R-matrix radius was assumed to be 5.4 au, and 25 continuum orbitals were included for each channel angular momentum for the expansion of the wave function. This made it possible to compute Ω up to an energy of 100 Ryd. In order to obtain convergence of Ω for all transitions and at all energies, all partial waves with angular momentum J up to 40.5 were included, and for higher partial waves an approximation was based on the Coulomb-Bethe approximation for allowed transitions and a geometric series for forbidden transitions. The collision strengths and effective collision strengths are presented in [20, 21] for all transitions among the 48 fine-structure levels.

Examples of collision strengths calculated in papers [16, 17, 19, 2, 20] are shown in Figures 17-23, and effective collision strengths [19, 2, 21] are presented in Figures 24-27.

From the comparison of collision strength values obtained in [16, 19, 2, 20] it can be seen that the differences between R-matrix calculations [20] and earlier DW calculations [16] are within 50%, and are in accordance with the corresponding oscillator strength values. Since in [16] configuration interaction was taken into account only for the basic configurations, results [16] for oscillator strengths and collision strengths are comparatively less accurate than [20]. Additionally, values of Ω were calculated in [16] at only three energies above thresholds; this is not sufficient for the accurate determination of excitation rates, as resonances in the thresholds region were not accounted for.

It should be noted that R-matrix results in [19, 2] differ up to a factor of 7 for some transitions and do not agree with other R-matrix [20] and DW [16] calculations for a few transitions. Because the f-values are not presented in [19, 2], it is difficult to understand the source of the discrepancy. Note, that CIV3 calculations give good results for f-values if 1523 configurations are taken into account [25]. However, in [19, 2] only a limited set of 123 configurations was used. This drastic reduction in the number of configurations (by over an order of magnitude) perhaps significantly altered the f-values, especially for the transitions with relatively small magnitudes. Therefore, we can suppose that the Ω values of [19, 2] are also comparatively less accurate. It should be also noted that in both calculations [16] and [19, 2] only partial waves with J up to 17.5 were included before invoking the contribution of higher neglected partial waves from the Coulomb-Bethe approximation. This range of partial waves is sufficient for the convergence of Ω in the energy range of their calculations for a majority of transitions. But, as shown in [20], for a few allowed transitions, and particularly towards the higher end of our energy range, this set of partial waves is not sufficient for convergence. It can be clearly seen from Figure 28 that, for example, for the 41–48 transition at energies > 20 Ryd a higher range of partial waves is desirable.

Effective collision strengths are obtained after integrating the Ω data over a Maxwellian distribution of electron velocities. Since the threshold region is dominated by numerous resonances, Ω must be computed on a fine energy mesh. In paper [21] the mesh was 0.001 Ryd close to thresholds and was 0.002 Ryd in the remaining range. In [18, 19,

2, 20] calculations, the mesh was 0.005 Ryd. Differences of a factor of two exist between the two R-matrix calculations [19, 2] and [21] for many transitions and in almost the entire temperature range. These were mainly due to better resolution of resonances in [21] and inclusion of higher range of energy for the calculations of Ω . Note, that in [19, 2] collision strengths were calculated up to an energy of 40 Ryd only, which is not sufficient for convergence of the integral for effective collision strengths, especially towards the higher end of their temperature range. As a result, values of Γ may be underestimated by up to a factor of two.

In paper of Wang et al. [26] relative values of the electron collisional excitation rate coefficients of Fe XI ion were measured using a theta pinch device. After that, Wang et al [27] deduced the absolute excitation rate coefficients of Fe XI ion from the relative measurements using the absolute excitation rate coefficients of the Fe X ion as a standard. Comparison of experimental and theoretical data at $T_e=160\text{eV}$ are shown in Figure 29. It can be seen from these figures that experimental accuracy $\sim 70\%$ is not good enough to estimate the accuracy of theoretical calculations. Taking experimental accuracy into consideration, we may state that theory and experiment agree satisfactory.

Thus we can conclude that at the present time the most accurate data on collision strengths and on effective collision strengths for transitions in S-like Fe (Fe XI) ion are presented in papers [20, 21] because these calculations: 1) have included configuration interaction among 235 configurations (123 in [18, 19, 2]); 2) are fully relativistic calculations in jj-coupling scheme; 3) have included partial waves up to $J = 40.5$ (17.5 in [18, 19, 2]), 4) have computed values of Ω up to 100 Ryd (40 Ryd in [18, 19, 2]); 5) have included resonances among 48 levels (38 in [18, 19, 2]); and 6) have used a fine energy mesh of better than 0.002 Ryd (0.005 Ryd in [18, 19, 2]). Authors of [20, 21] estimated the accuracy of their calculations as better than 10% at energies below 25 Ryd for all transitions and as better than 20% at higher energies for a few allowed transitions. It should be noted that in the CHIANTI atomic database less accurate data [18, 19, 2] are used, while we recommend to use for the first 48 levels data [20, 21].

2.3 Excitation of $n=3 - n'=3$ transitions in Si-like Fe XIII by electron impact.

In the past 20 years a variety of calculations have been performed to compute various atomic parameters of Fe XIII ion. The most notable ones among the available data,

particularly for collision strengths Ω and effective collision strengths Γ , are the calculations carried out by Fawcett & Mason [28], Tayal [2, 29], Gupta & Tayal [30] and Aggarwal & Keenan [31, 32].

Fawcett & Mason [28] have used for the Slater parameter optimization method. This method was realized with the following suite of atomic codes: 1) distorted wave program (DSTWAV) of Eissner & Seaton [6, 33], which computes collision strengths and reactance matrices in *LS* coupling, 2) atomic-structure program SUPERSTRUCTURE of Eissner et al [5], 3) the JAJOM code of Saraph [34, 7], which uses term-coupling coefficients from SUPERSTRUCTURE and reactance matrices from DSTWAV and makes the transformation to collision strengths between fine-structure levels, and 4) least-squares-fitting routine (RCE) from the Hartree-Fock-Relativistic (HFR) atomic-structure code of Cowan [35-37], which was used for optimization of Slater parameters. The Slater parameters (the centers-of-gravity energy for all configurations, the single-configuration direct and exchange Coulomb-interaction radial integrals, the spin-orbit parameters, and the configuration-interaction integrals) were first computed *ab initio* with the HFR code and subsequently adjusted with the least-squares optimization routines RCE on the basis of minimizing the discrepancies between observed and computed energy levels. Six configurations, $3s^23p^2$, $3p^4$, $3s3p^3$, $3s^23p3d$, $3s3p3d^2$, and $3p^33d$, were included in these collision computations; hence configuration-interaction problems are more comprehensively dealt with than for previously published Fe XIII computations [38, 39]. The Fe XIII collision strengths for $3s^23p^2$ - $3s3p^3$ and $3s^23p^2$ - $3s^23p3d$ transitions were presented by Fawcett & Mason for the three electron energies 15.0, 30.0, and 45.0 Ryd. These collision strengths were calculated for partial waves of angular momentum $L = 0 - 7$ and with the Bethe approximation technique developed by Burgess & Sheorey [22] for partial waves $L = 8$ to infinity.

Unfortunately, Fawcett & Mason [28] presented the values of Ω at only 3 energies above thresholds, and resonances in the thresholds region were not taken into account. Therefore, any results obtained for Γ from limited data of Ω will be underestimated by up to an order of magnitude, especially for the forbidden transitions. The second limitation of calculations [28] is using of Bethe approximation to calculate collision strengths for partial waves with $L \geq 8$, because Bethe approximation may overestimate Ω for such low partial waves.

Attempts to remove both the limitations of above calculations were done by Tayal [2, 29] and Gupta & Tayal [30]. In papers [2, 29, 30] extensive semirelativistic R-matrix calculation for electron impact excitation of Fe XIII by including electron correlation, relativistic, and resonance effects were carried out. The relativistic effects were included in the Breit-Pauli approximation via the one-body mass correction, Darwin, and spin-orbit interaction terms in the scattering equations. In these works, 26 fine-structure levels of the configurations $3s^23p^2$, $3s3p^3$, and $3s^23p3d$ in Fe XIII were considered, which were represented by configuration interaction wave functions. For the generation of wave functions ten orthogonal orbitals 1s, 2s, 3s, 4s, 2p, 3p, 4p, 3d, 4d, and 4f were included, and resonances were resolved in order to improve the accuracy of the Γ results. CIV3 program [8] was applied for the generation of wave functions. The full Breit-Pauli R-matrix calculations by codes of [40, 9] were performed to calculate partial collision strengths from $J = 0.5$ to $J = 22.5$. The contribution from higher partial waves was calculated using the Coulomb-Bethe approximation for dipole-allowed transitions and was estimated using a top-up for the nondipole transitions. A fine energy mesh of 0.005 Ryd was used in the threshold energy regions to account for the resonance structures. It was shown that complicated resonance structures enhance collision strengths significantly for many transitions.

The main limitations of calculations [2, 29, 30] are: 1) using of earlier version of the R-matrix code [41] which is known to have some errors, 2) energy mesh 0.005 Ryd is not enough fine for correct consideration of resonances, 3) only 28 lower levels are considered, resonances arising from the higher levels are not included, and 4) Ω is computed up to $E = 60$ Ryd, which is not sufficient for the convergence of the integral for effective collision strength.

We note that the calculations of Fawcett & Mason [28] and Tayal [2, 29] and Gupta & Tayal [30] have been used for plasma kinetic modeling, but, as shown recently by Landi [42], give results different by a factor of 2 for measured values of plasma density.

In the most recent calculations of Aggarwal & Keenan [31, 32] a fully relativistic approach based on the GRASP code of Dyall et al. [10] for the generation of wave functions, and the Dirac Atomic R-matrix Code (DARC) of Norrington & Grant (2006, to be published) for the computation of collision and effective collision strengths have been

used. In these papers 97 fine structure levels of configurations $3s^23p^2$, $3s3p^3$, $3s^23p3d$, $3p^4$, $3s3p^23d$ and $3s^23d^2$ were taken into account and, consequently, for the first time resonances arising from the higher lying levels, mainly from the $3p^4$, $3s3p^23d$ and $3s^23d^2$ configurations, were considered. Additionally relativistic effects were fully taken into account, unlike earlier calculations [2, 29, 30] which neglected the two-body relativistic operators. The R-matrix radius in the calculations [31, 32] was adopted to be 3.0 au, and 15 continuum orbitals were included for each channel angular momentum for the expansion of the wave function. This made it possible to compute Ω up to an energy of 120 Ryd. The maximum number of channels for one partial wave was 475, and the corresponding size of the Hamiltonian matrix was 7138. In order to obtain convergence of Ω for all transitions and at all energies, all partial waves with angular momentum $J \leq 39.5$ have been included, and a top-up procedure, based on the Coulomb-Bethe approximation for allowed transitions and geometric series for forbidden transitions was used for higher partial waves. In Figs. 30 and 31 the variations of Ω with angular momentum J , calculated in paper [31], are shown for forbidden transitions $3s^23p^2 \ ^3P_1-3s^23p^2 \ ^3P_2$ and allowed transition $3s^23p^2 \ ^3P_1-3s^23p3d \ ^3D_1$.

It can be seen that for forbidden transitions the values of Ω are fully converged including the highest energy of 120 Ryd. However, it is clear from figure 31 that for allowed transition the values of Ω fully converged within the partial waves range $J \leq 39.5$ only at energies below 45 Ryd, and even this large range of partial waves is not sufficient for the convergence of Ω at higher energies.

The examples of comparison of the collision strengths calculated in papers [28, 30, 31] are shown in Figures 32 and 33, and comparison of the effective collision strengths of [2, 30, 32] are presented in Figures 34 - 37 for the most important transitions mentioned above.

As was shown by Aggarwal & Keenan [31], the results of [28] for Ω are small for almost all transitions. This is mainly because only a limited range of partial waves $L \leq 7$ was considered in paper [28]. This limited range of partial waves is not sufficient for the convergence of Ω for forbidden transitions and the Coulomb-Bethe approximation is inadequate for the neglected higher partial waves. As a result of this, the values of Ω from [28] are underestimated for the forbidden transitions and overestimated for the allowed transitions. The results of [30] for Ω are in broad agreement with DARC calculations in

[31], although serious differences exist for a few forbidden transitions. This is probably explained by some errors in the earlier version of the R-matrix program [41].

The agreement between the effective collision strengths calculated in papers [2, 30] and [32] is worse: the differences vary from a few percent to over an order of magnitude for a majority of the transitions (see, for example, Fig. 33). Analysis carried out by Aggarwal & Keenan [32] shows that there are two types of differences between the two sets of results [2, 30] and [32].

There are transitions for which the differences are largest at the lowest temperature, and they decrease with increasing temperature (see transitions ${}^3P_0-{}^3P_1$, ${}^3P_0-{}^3P_2$, ${}^3P_1-{}^3P_2$ in Fig. 34). For such transitions the difference is caused by large resonances in the threshold region. This region is more accurately considered in work [32], because, first, the energy mesh in these calculations is finer (better than 0.002 Ryd) in comparison to the coarse mesh of 0.005 Ryd of [2, 30] and, second, the calculations of [2, 30] are restricted to the lowest 28 levels, whereas calculations [31, 32] include 97 levels (as a result of this, resonances arising from the higher levels were not included in calculations [2, 30]).

For some transitions, such as ${}^3P_0-{}^1S_0$ or ${}^1D_2-{}^1S_0$, differences in the two sets of Γ persist throughout the entire range of temperature. These differences are partly due to the factors discussed above, but partly are caused by another reason. In papers [2, 30] the values of Γ are presented up to a temperature of 5×10^6 K, which corresponds to 32 Ryd in energy units. However, the values of Ω were calculated up to energy of 60 Ryd only, which is not sufficient for the convergence of the integral for effective collision strength, particularly for higher temperatures. As a result of this, the values of Γ from [2, 30] are underestimated towards the higher end of the temperature range. This can be easily verified by a closer look at results of [2, 30] for Ω and Γ shown in Fig. 33 for the transition $3s^23p^2 {}^3P_1-3s^23p3d {}^3D_0$. As expected for allowed transitions, results for Ω increase with increasing energy in sets of calculations [2, 30] and [31, 32], but the behavior of Γ is exactly opposite. The results for Γ of [32] increase with increasing temperature, whereas those of [2] decrease. Thus it is possible to conclude that Γ values presented in [2, 30], and adopted by Landi [42], are deficient for many transitions.

Thus, the analysis carried out above shows that at the present time the most accurate and reliable results for the effective collision strengths for the transitions in

Si-like Fe (Fe XIII) ions are obtained by Aggarwal & Keenan [32]. The calculations are fully relativistic in the jj-coupling scheme and include 1) a larger number of fine-structure levels (97 in comparison to the 26); 2) a wider range of partial waves ($J \leq 39.5$ in comparison to the $J \leq 22.5$); 3) a higher range of energy (120 Ryd in comparison to the 60 Ryd); 4) improved Γ values by resolving resonances in a finer energy mesh (better 0.002 Ryd in comparison to the 0.005 Ryd); and 5) additional levels among which the transitions have already been observed. We recommend to use these data [32] in Fe XIII kinetic calculations.

3. Analytical functions for approximation of dependencies of effective collisional strengths on electron temperature.

It was noted above that for many applications it is desirable to have analytical dependences of effective collision strengths on electron temperature. To obtain such analytical dependences it is possible to use some universal functions $f_k(T_e, p_1, p_2, \dots)$ depending on T_e and on the finite number of free parameters p_1, p_2, \dots and to determine the values of p_j for each collisional transition. This determination may be based on minimization of some object function describing the difference between $\Gamma_{ij}(T_e)$ and $f_k(T_e, p_1, p_2, \dots)$. Usually the following object function is used:

$$F(p_1, p_2, \dots) = \sum_{T_e} (\Gamma(T_e) - f(T_e, p_1, p_2, \dots))^2 \quad (1)$$

and just this function was minimized in the present work to obtain values of free parameters p_j for all considered collisional transitions.

As function f_k we have used 3 simple functions depending on 7 free parameters:

$$f_1(x, p_1, p_2, p_3, p_4, p_5, p_6, p_7) = p_1 \frac{\exp(-(p_2/x)^{p_3})}{1 + (x/p_4)^{p_5} + (x/p_6)^{p_7}} \quad (2)$$

$$f_2(x, p_1, p_2, p_3, p_4, p_5, p_6, p_7) = p_1 \frac{\exp(-(p_2/x)^{p_3})}{1 - (x/p_4)^{p_5} + (x/p_6)^{p_7}} \quad (3)$$

$$f_3(x, p_1, p_2, p_3, p_4, p_5, p_6, p_7) = p_1 \exp(-(p_2/x)^{p_3}) (1 + (p_4/x)^{p_5} + (x/p_6)^{p_7}) \quad (4)$$

By minimizing of expression (1) we have obtained values of parameters $p_1, p_2, p_3, p_4, p_5, p_6,$ and p_7 for all transitions considered above. The accuracy of the approximations

ranges from 1% to 13%. For the most part of transitions the approximation accuracy is better than 5%. The values of parameters p_i for electron impact excitation of $n=3 - n'=3$ transitions in Fe X, XI, XIII ions will be available from the NIFS atomic database [43].

4. Summary.

In the present work we carried out the comparison of data obtained for electron-induced excitation transitions between levels with principal quantum numbers $n=3$ in Fe X, XI, XIII ions by different theoretical methods, and chose recommended data for electron collision strengths and effective collision strength. Simple analytical formulas with 7 free parameters were used to describe electron temperature dependence of effective collision strengths in a wide temperature range. The values of free parameters have been determined by fitting a formula with recommended numerical data and have been inputted into NIFS atomic database. The results obtained can be used for plasma kinetics calculations and for development of spectroscopic methods of plasma diagnostics.

Acknowledgement

This work was performed when I. S. was a visiting professor at the National Institute for Fusion Science from Sep. 2005 to Jan. 2006. We are grateful to Prof. R. M. More for checking the manuscript.

References

1. A. K. Bhatia, G. A. Doschek, *At. Data Nucl. Data Tables*, **60**, 97 (1995)
2. S. S. Tayal, *ApJ*, **544**, 575 (2000), *ApJS*, **132**, 117 (2001)
3. J. C Pelan, K. A. Berrington, *A&A*, **365**, 258 (2001)
4. K. M. Aggarwal, F. P. Keenan, *A&A*, **439**, 1215 (2005)
5. W. Eissner, M. Jones, H. Nussbaumer, *Comput. Phys. Commun.*, **8**, 270 (1974)
6. W. Eissner, M. J. Seaton, *J. Phys. B*, **5**, 2187 (1972)
7. H. E. Saraph, *Comput. Phys. Commun.*, **3**, 256 (1972)
8. A. Hibbert, *Comput. Phys. Commun.*, **9**, 141 (1975)
9. K. A. Berrington, W B. Eissner, P. H. Norrington, *Comput. Phys. Commun.*, **92**, 290 (1995)
10. K. G. Dyall, I. P. Grant, C. T. Johnson, F. A. Parpia, E. P. Plummer, *Comput. Phys. Commun.*, **55**, 424 (1989)
11. P. H. Norrington, I. P. Grant, *Comput. Phys. Commun.*, 2006 (to be published)
12. M. Mohan, A. Hibbert, A.E. Kingston, *ApJ*, **434**, 389 (1994)
13. J. S. Wang, H. R. Griem, *Phys. Rev.*, **A27**, 2249 (1983)
14. M. Malinovsky, J. Dubau, S. Sahal-Breshot, *ApJ*, **235**, 665 (1980)
15. G. Del Zanna, K.A. Berrington, and H.E. Mason, *A&A*, **422**, 731 (2004)
16. A. K. Bhatia, G. A. Doschek, *At. Data Nucl. Data Tables*, **64**, 183 (1996)
17. H. E. Mason, *Mon. Not. R. Astron. Soc.* **170**, 651 (1975)
18. G. P. Gupta, S. S. Tayal, *ApJ*, **510**, 1078 (1999)
19. G. P. Gupta, S. S. Tayal, S. S., *ApJSS*, **123**, 295 (1999)
20. K. M. Aggarwal, F. P. Keenan, *MNRAS*, **338**, 412 (2003)
21. K. M. Aggarwal, F. P. Keenan, *A&A*, **399**, 799 (2003)
22. A. Burgess and V. B. Sheorey, *J. Phys. B*, **7**, 2403 (1974)
23. N. S. Scott, P. G. Burke, *J. Phys. B*, **13**, 4299 (1980)
24. E. Clementi, C. Roetti, *At. Data Nucl. Data Tables*, **14**, 177 (1974)
25. N. C. Deb, S. S. Tayal, *At. Data Nucl. Data Tables*, **69**, 161 (1998)
26. J. S. Wang, , A. Marotta, U. D. Raju, *ApJS*, **279**, 460 (1984)
27. J. S. Wang, U. D. Raju, H. R. Griem, *Phys. Rev. A*, **29**,1558 (1984)
28. B. C. Fawcett, H. E. Mason, *ADNDT*, **43**, 245 (1989)
29. S. S Tayal, *ApJ*, **446**, 895 (1995)

30. G. P. Gupta, S. S. Tayal, *ApJ*, 506, 464 (1998)
31. K. M. Aggarwal, F. P. Keenan, *A&A*, 418, 371 (2004)
32. K. M. Aggarwal, F. P. Keenan, *A&A*, 429, 1117 (2005)
33. P. G. Burke and W. E. Eissner, in *Atoms in Astrophysics Chap. I* (Plenum, New York, 1983)
34. H. E. Saraph, *Comput. Phys. Commun.*, 1,232 (1970)
35. R. D. Cowan, *The Theory of Atomic Structure and Spectra* (Univ. of California Press, Los Angeles, 1981)
36. R. D. Cowan, *JOSA*, 58, 808, 924 (1968)
37. R. D. Cowan and D. C Griffin, *JOSA*, 65, 1010 (1976)
38. D. R. Flower and G. Pineau Des Forets, *A&A*, 24, 181 (1973)
39. D. R. Flower and H. Nussbaumer, *A&A*, 31, 353 (1974)
40. K. A. Berrington, P. G. Burke, K. Butler, M. J. Seaton, P. J. Storey, K. T. Taylor, Y. Yu, *J. Phys. B*, 20, 6379 (1987)
41. N. S. Scott, K. T. Taylor, *Comput. Phys. Commun.*, 25, 347 (1982)
42. E. Landi, *A&A*, 382, 1106 (2002)
43. NIFS Database, <http://dbshino.nifs.ac.jp/>

Table 1. Comparison of measured values of energies of excited levels of Fe X ion with calculated ones.

N	Configuration	Term	Energy, Exp, Ry	$(E_{\text{calc}}-E_{\text{exp}})/E_{\text{exp}} \cdot 100\%$				
				[1]	[2]	[3]	[12]	[4]
2	$3s^23p^5$	$^2P_{1/2}$	0.142915	-7.49	-6.08	-5.82	-100	-0.22
3	$3s3p^6$	$^2S_{1/2}$	2.635831	-0.11	-0.63	-0.18	-6.86	-1.27
4	$3s^23p^4(^3P)3d$	$^4D_{5/2}$	3.542177	0.40	1.75	1.10	-2.10	0.14
6	$3s^23p^4(^3P)3d$	$^4D_{3/2}$	3.554397	0.33	1.67	1.03	-2.44	0.12
11	$3s^23p^4(^3P)3d$	$^4F_{5/2}$	3.888951	0.30	2.74	1.26	-2.88	0.85
27	$3s^23p^4(^1D)3d$	$^2S_{1/2}$	4.937965	6.86	2.01	2.45	5.41	1.72
28	$3s^23p^4(^3P)3d$	$^2P_{3/2}$	5.14135	3.51	4.06	2.21	2.63	2.55
29	$3s^23p^4(^3P)3d$	$^2P_{1/2}$	5.194086	3.51	3.93	2.17	1.58	2.51
30	$3s^23p^4(^3P)3d$	$^2D_{5/2}$	5.221141	4.81	4.86	2.49	4.46	2.33
31	$3s^23p^4(^3P)3d$	$^2D_{3/2}$	5.342248	4.56	4.57	2.32	2.09	2.27

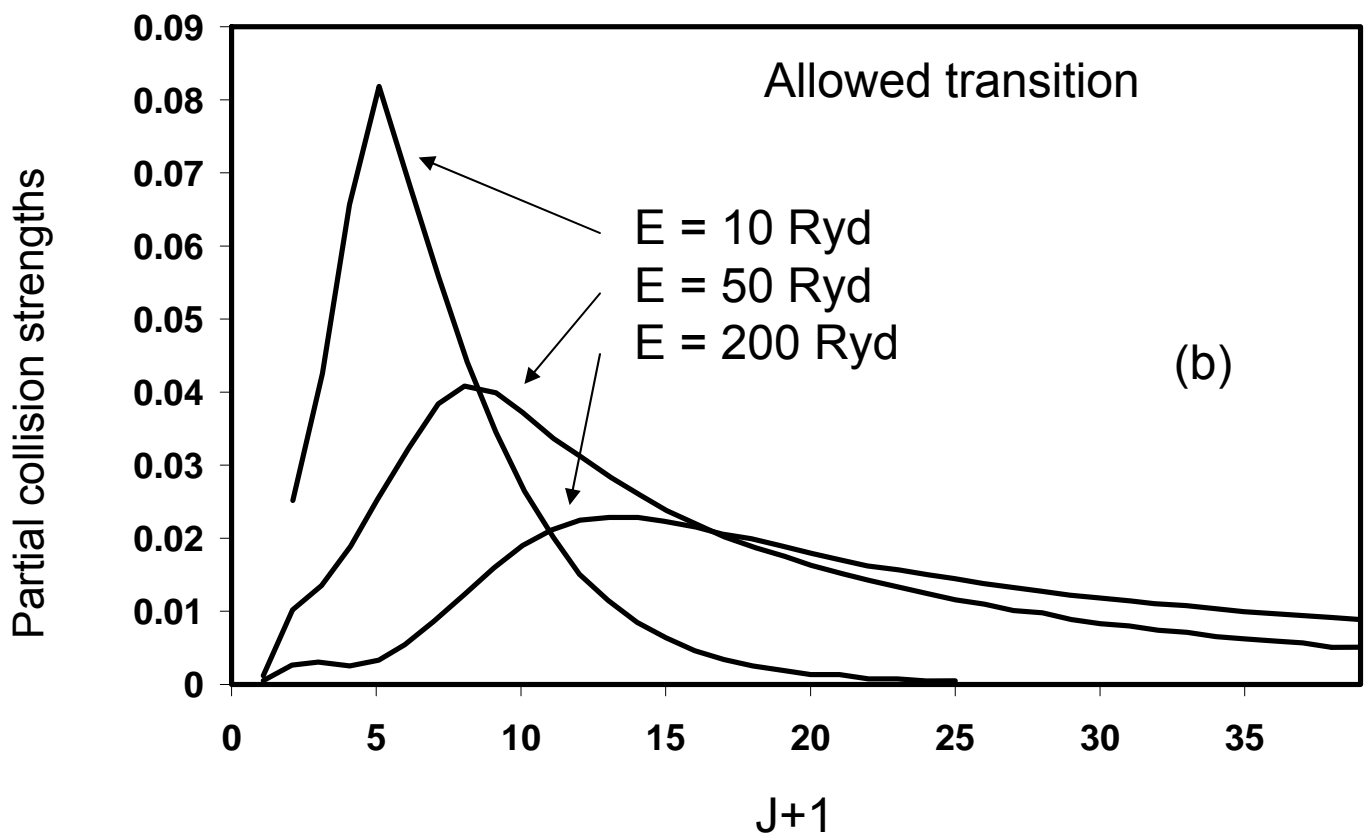
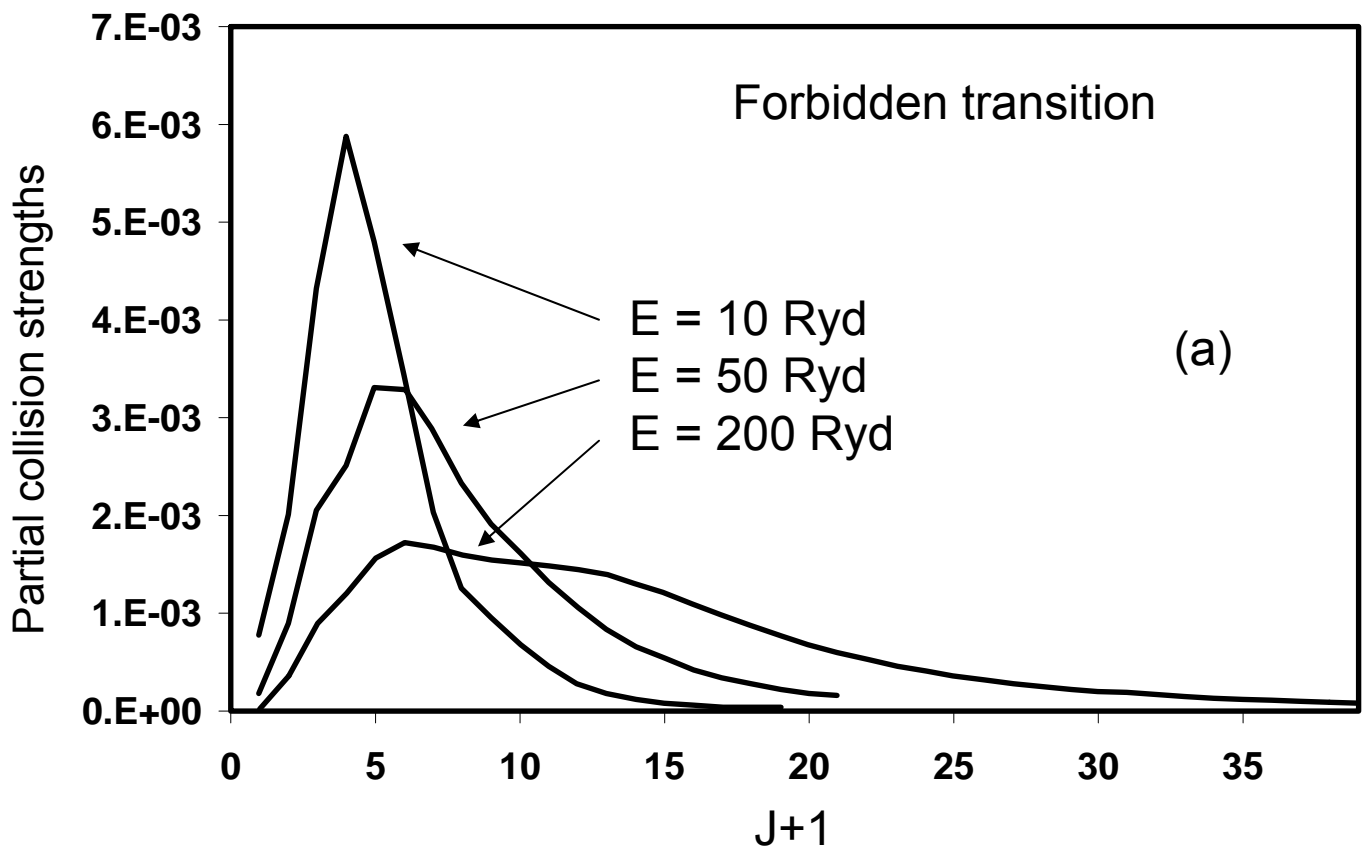


Figure 1. Partial collision strengths for (a) $3s3p^6\ ^2S_{1/2} - 3s^23p^4(^1S)3d\ ^2D_{5/2}$, and (b) $3s^23p^5\ ^2P_{3/2} - 3s3p^6\ ^2S_{1/2}$ transitions of Fe X at three energies of 10 Ryd, 50 Ryd and 200 Ryd.

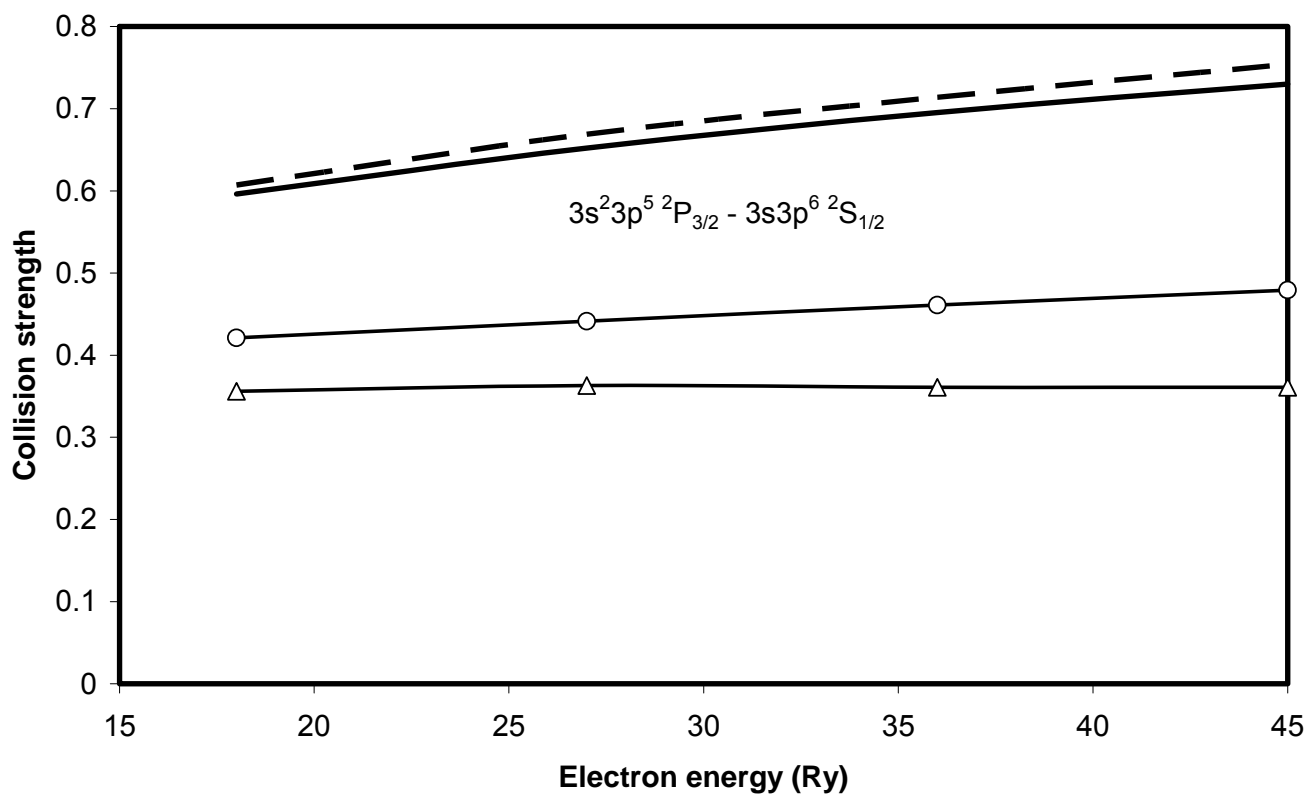


Figure 2. Comparison of collision strength, calculated in for transition $3s^2 3p^5 \ ^2P_{3/2} - 3s 3p^6 \ ^2S_{1/2}$ of Fe X: solid line – [4], dashed line – [2], solid line with Δ - [3], solid line with \circ - [1].

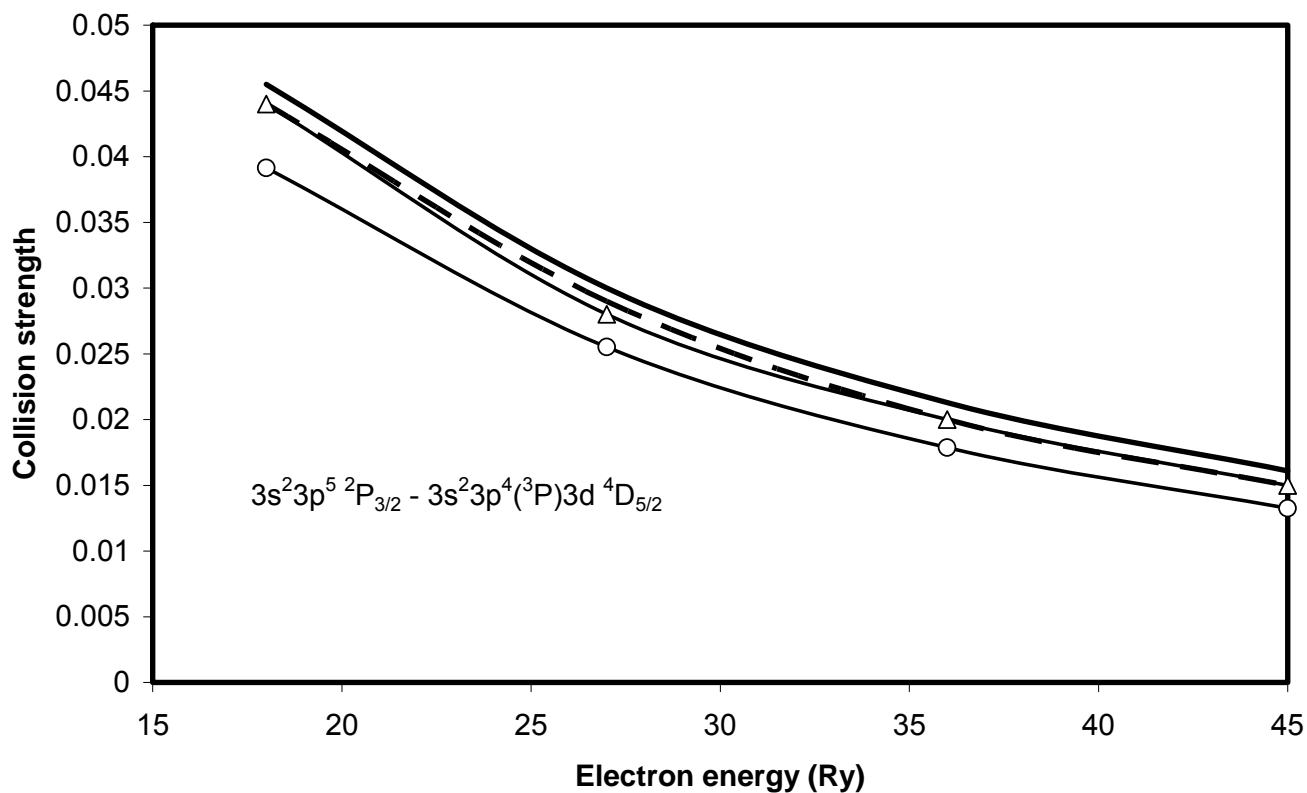


Figure 3. Comparison of collision strength, calculated for transition $3s^2 3p^5 \ ^2P_{3/2} - 3s^2 3p^4 (^3P) 3d \ ^4D_{5/2}$ of Fe X: solid line – [4], dashed line – [2], solid line with Δ - [3], solid line with \circ - [1].

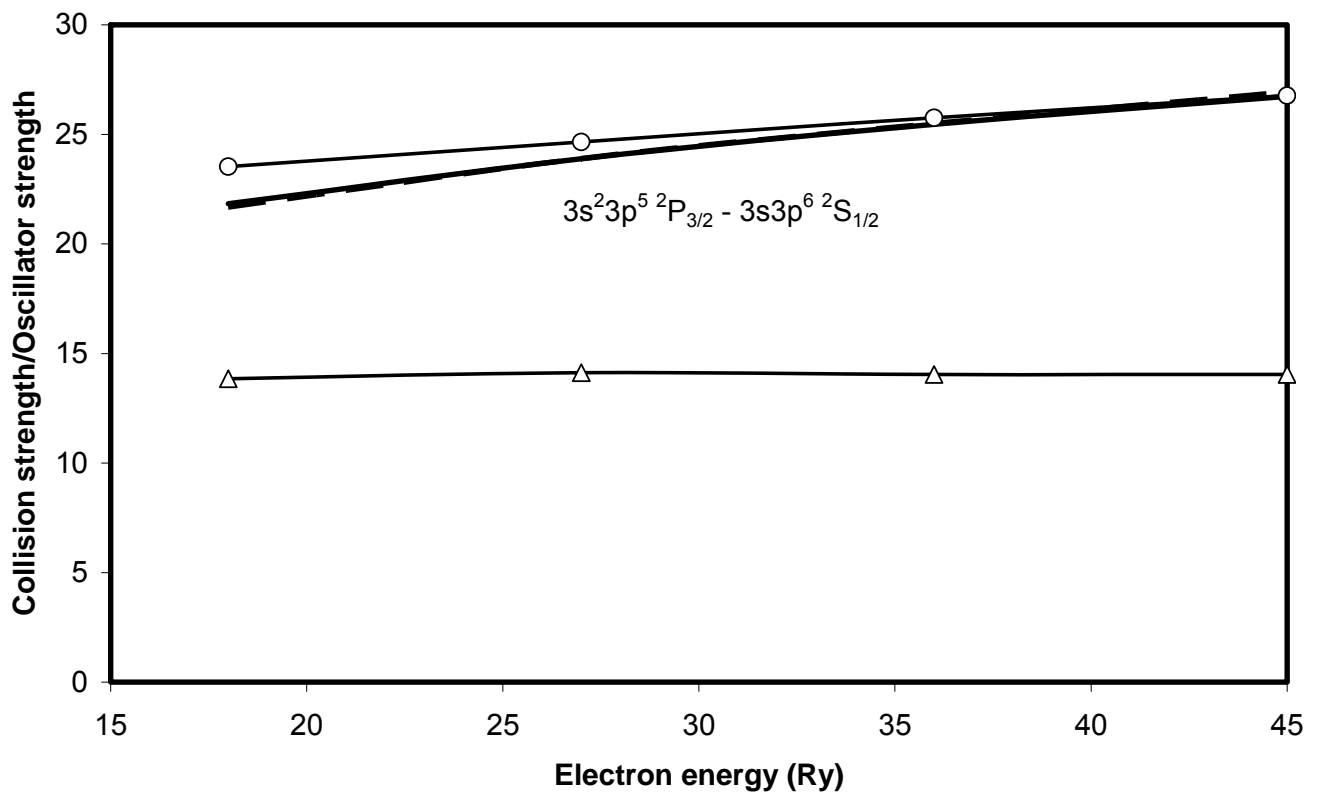


Figure 4. Comparison of ratio of collision strength to oscillator strength, calculated for transition $3s^2 3p^5 2P_{3/2} - 3s 3p^6 2S_{1/2}$ of Fe X: solid line – [4], dashed line – [2], solid line with Δ - [3], solid line with \circ - [1].

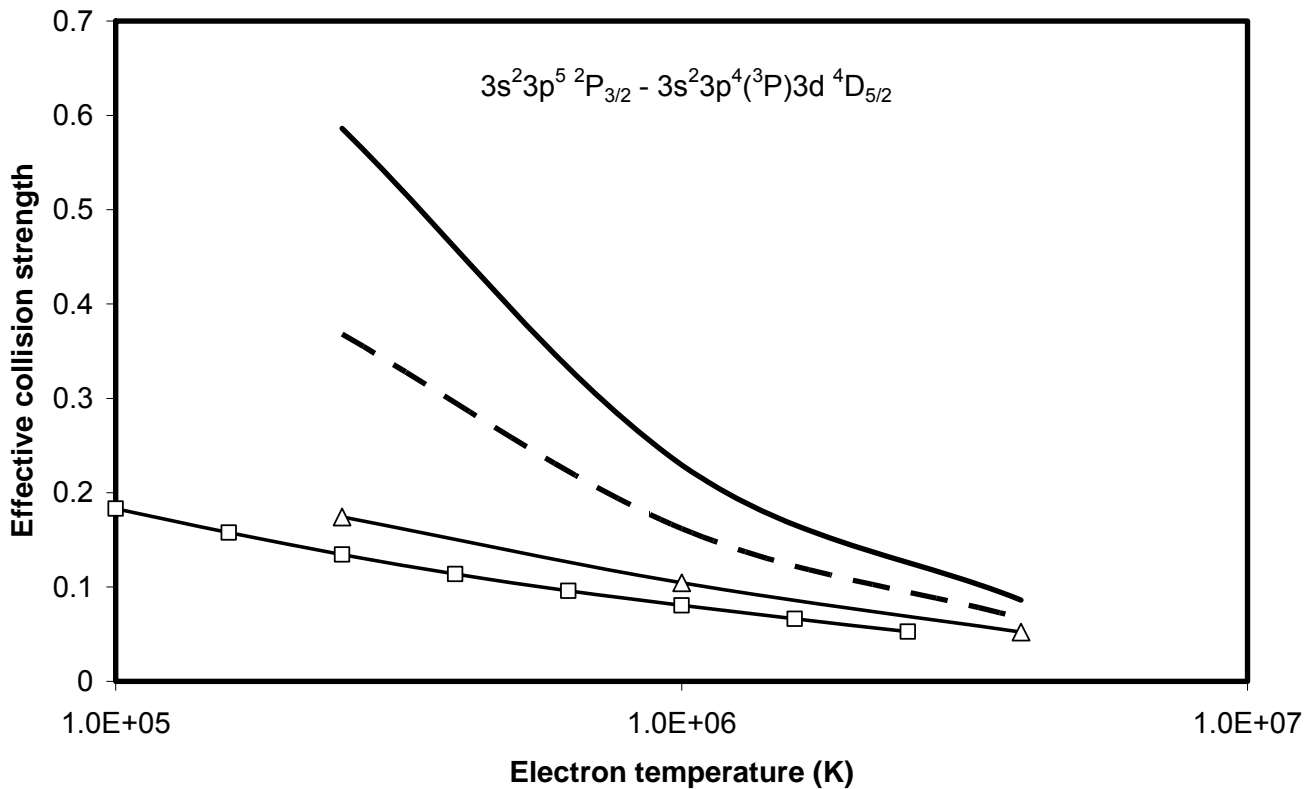


Figure 5. Comparison of effective collision strength, calculated for transition $3s^2 3p^5 2P_{3/2} - 3s^2 3p^4 (3P) 3d 4D_{5/2}$ of Fe X: solid line – [4], dashed line – [2], solid line with Δ - [3], solid line with \square - [12].

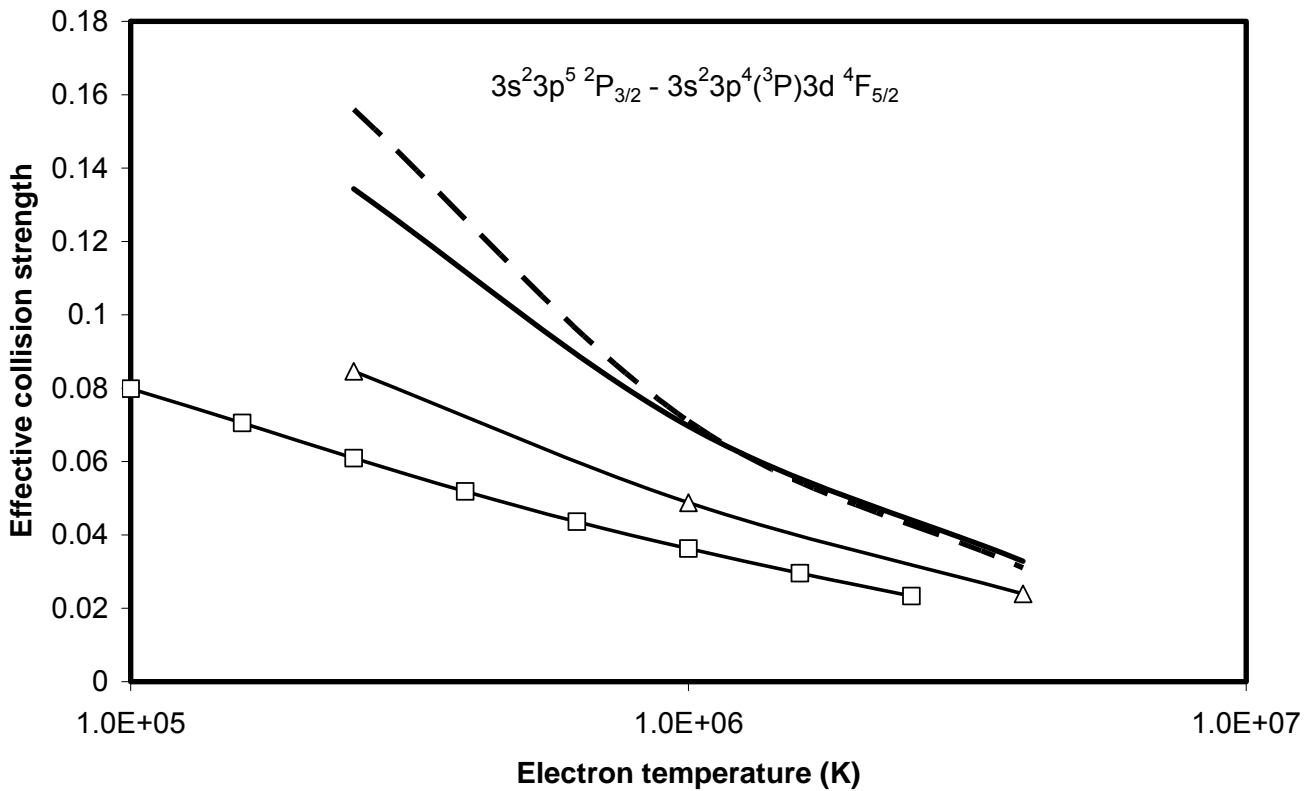


Figure 6. Comparison of effective collision strength, calculated for transition $3s^2 3p^5 \ ^2P_{3/2} - 3s^2 3p^4 (^3P) 3d \ ^4F_{5/2}$ of Fe X: solid line – [4], dashed line – [2], solid line with Δ - [3], solid line with \square - [12].

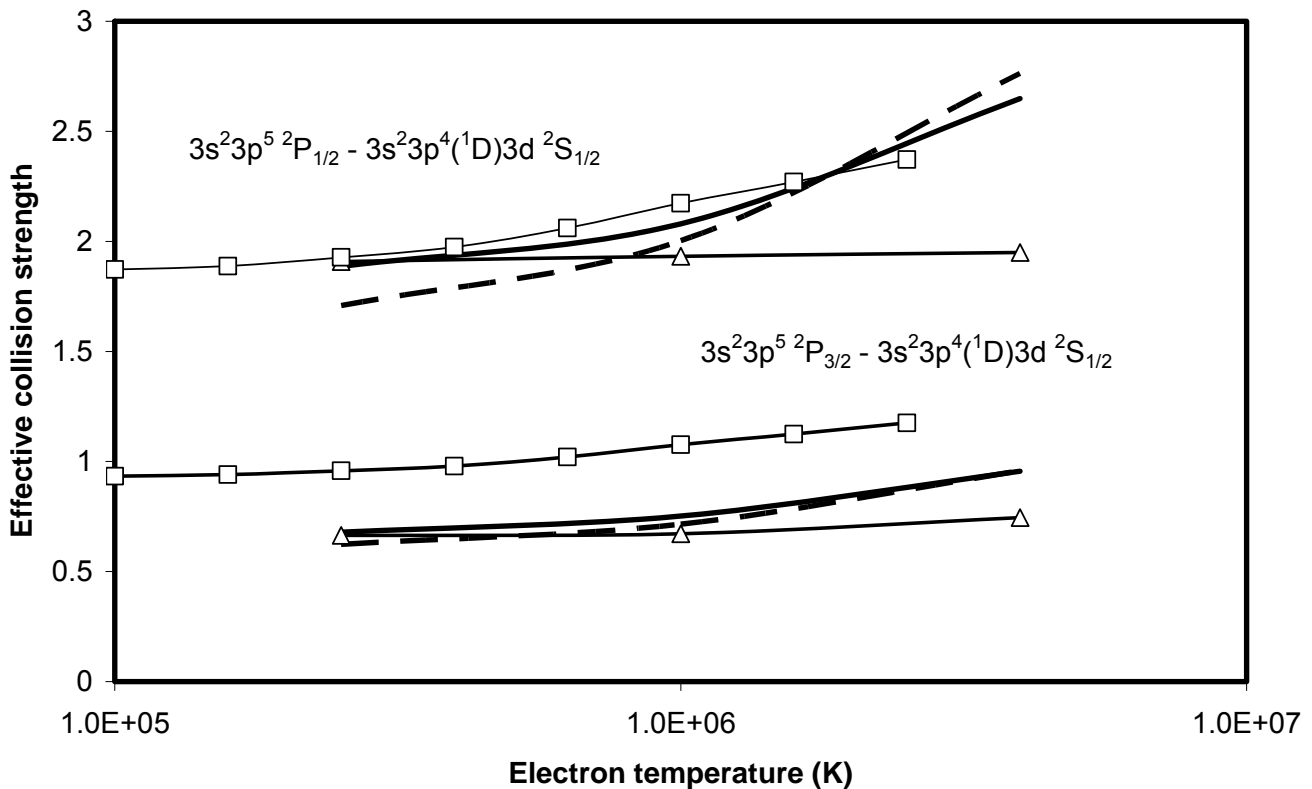


Figure 7. Comparison of effective collision strengths, calculated for transitions $3s^2 3p^5 \ ^2P_{3/2} - 3s^2 3p^4 (^1D) 3d \ ^2S_{1/2}$ and $3s^2 3p^5 \ ^2P_{1/2} - 3s^2 3p^4 (^1D) 3d \ ^2S_{1/2}$ of Fe X: solid line – [4], dashed line – [2], solid line with Δ - [3], solid line with \square - [12].

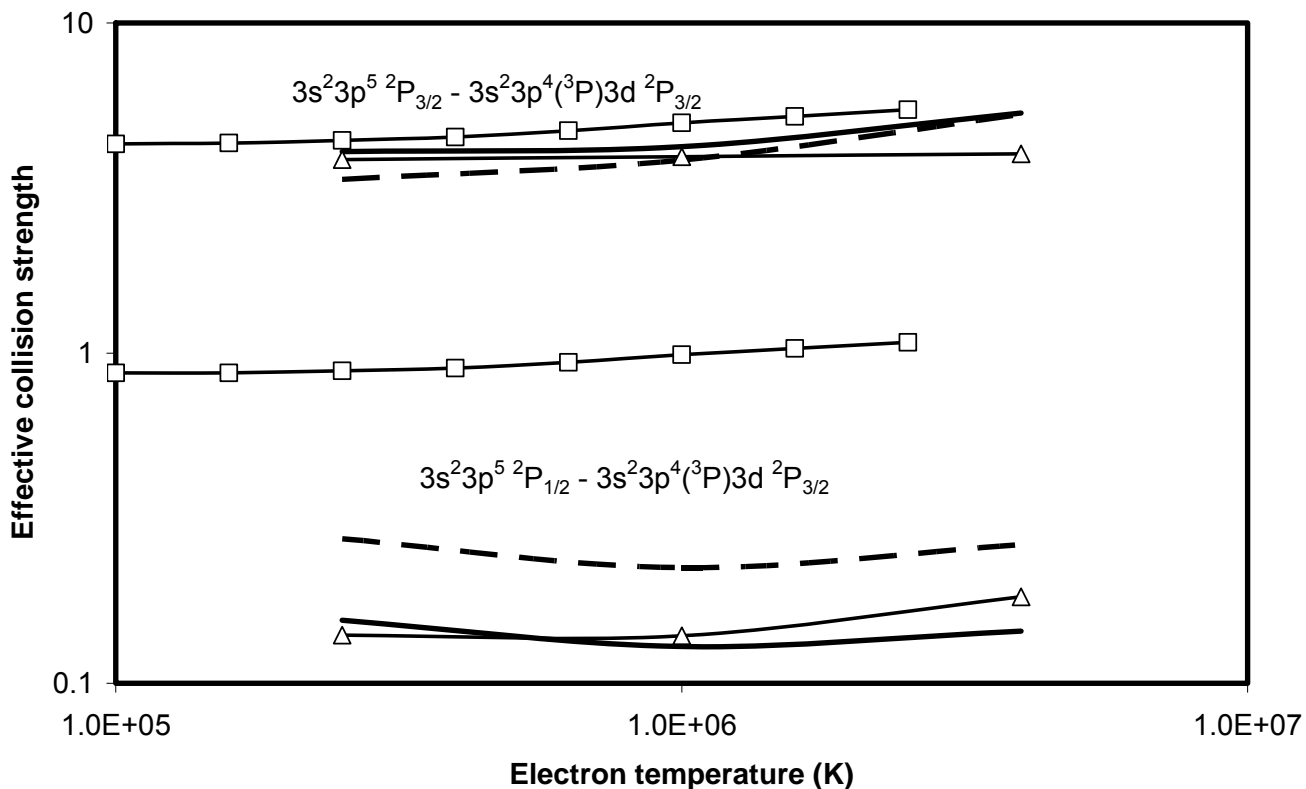


Figure 8. Comparison of effective collision strengths, calculated for transitions $3s^2 3p^5 \ ^2P_{3/2} - 3s^2 3p^4 (^3P) 3d^2 P_{3/2}$ and $3s^2 3p^5 \ ^2P_{1/2} - 3s^2 3p^4 (^3P) 3d^2 P_{3/2}$ of Fe X: solid line – [4], dashed line – [2], solid line with Δ – [3], solid line with \square – [12].

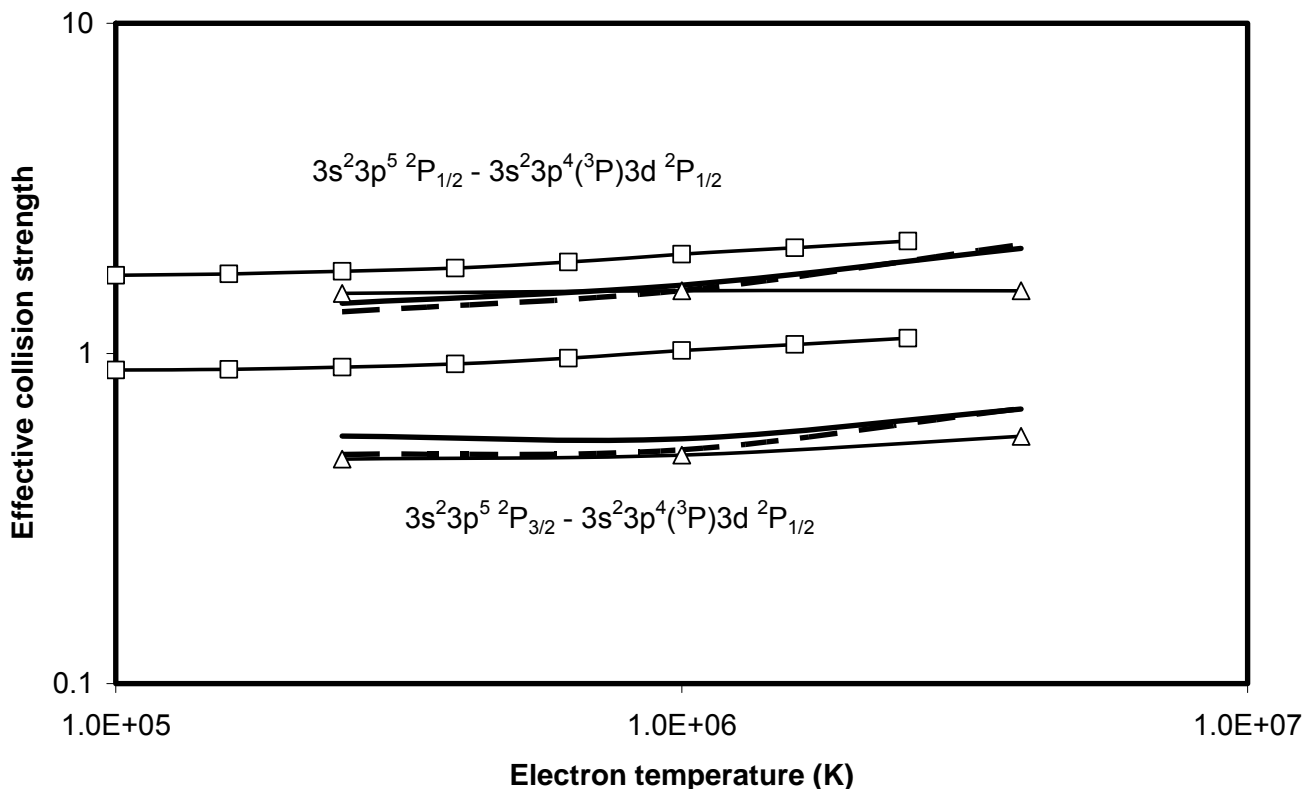


Figure 9. Comparison of effective collision strengths, calculated for transitions $3s^2 3p^5 \ ^2P_{3/2} - 3s^2 3p^4 (^3P) 3d^2 P_{1/2}$ and $3s^2 3p^5 \ ^2P_{1/2} - 3s^2 3p^4 (^3P) 3d^2 P_{1/2}$ of Fe X: solid line – [4], dashed line – [2], solid line with Δ – [3], solid line with \square – [12].

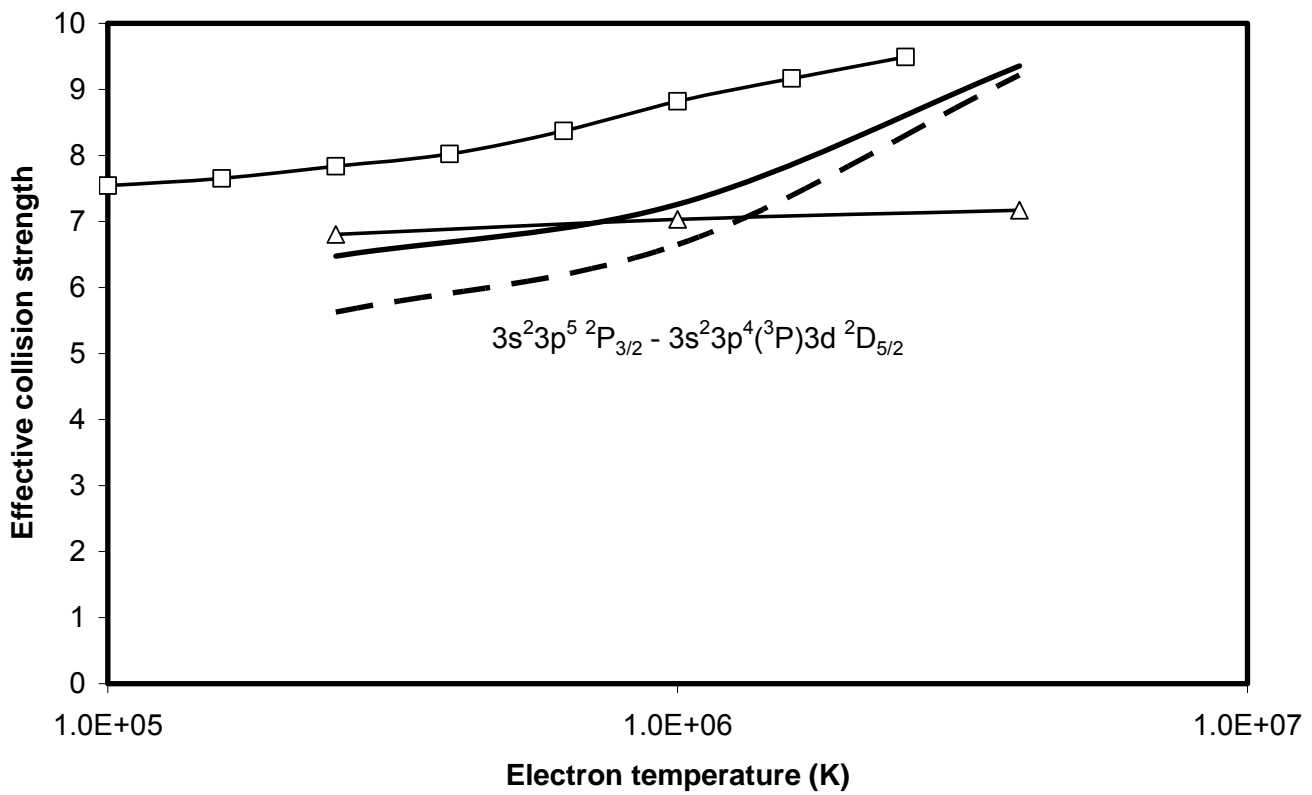


Figure 10. Comparison of effective collision strength, calculated for transition $3s^2 3p^5 \ ^2P_{3/2} - 3s^2 3p^4 (^3P) 3d \ ^2D_{5/2}$ of Fe X: solid line – [4], dashed line – [2], solid line with Δ - [3], solid line with \square - [12].

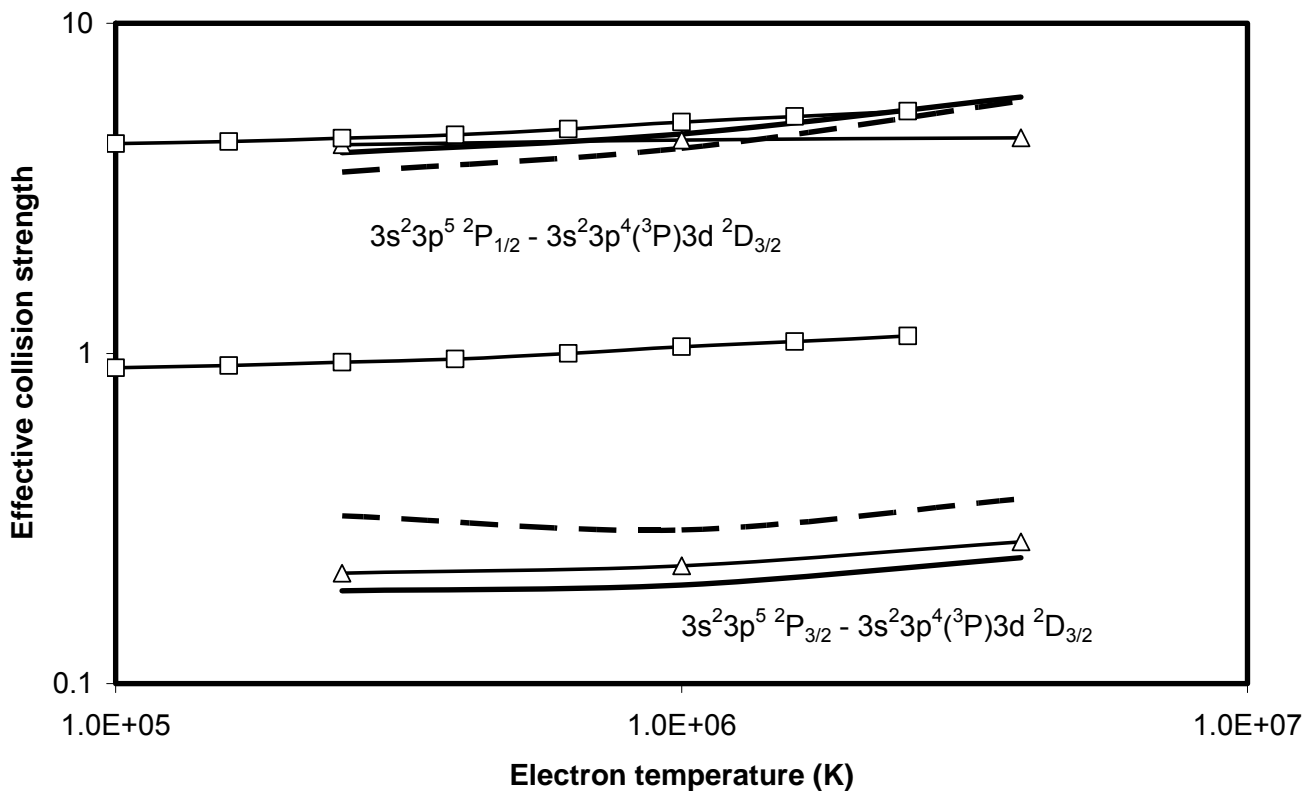


Figure 11. Comparison of effective collision strengths, calculated in for transitions $3s^2 3p^5 \ ^2P_{3/2} - 3s^2 3p^4 (^3P) 3d \ ^2D_{3/2}$ and $3s^2 3p^5 \ ^2P_{1/2} - 3s^2 3p^4 (^3P) 3d \ ^2D_{3/2}$ of Fe X: solid line – [4], dashed line – [2], solid line with Δ - [3], solid line with \square - [12].

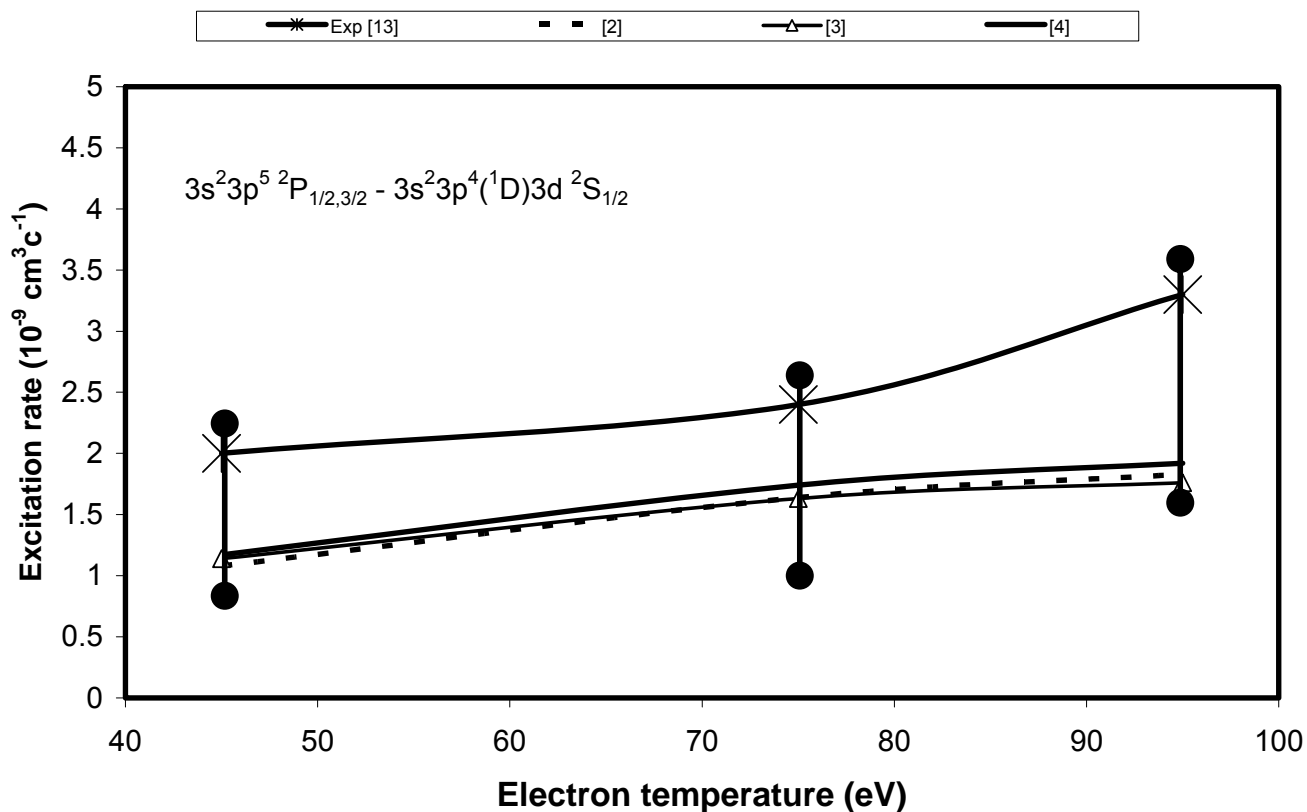


Figure 12. Comparison of experimental and theoretical excitation rates for transition $3s^2 3p^5 \ ^2P_{1/2,3/2} - 3s^2 3p^4 (^1D) 3d \ ^2S_{1/2}$ of Fe X: solid line – [4], dotted line – [2], solid line with * - experiment [13].

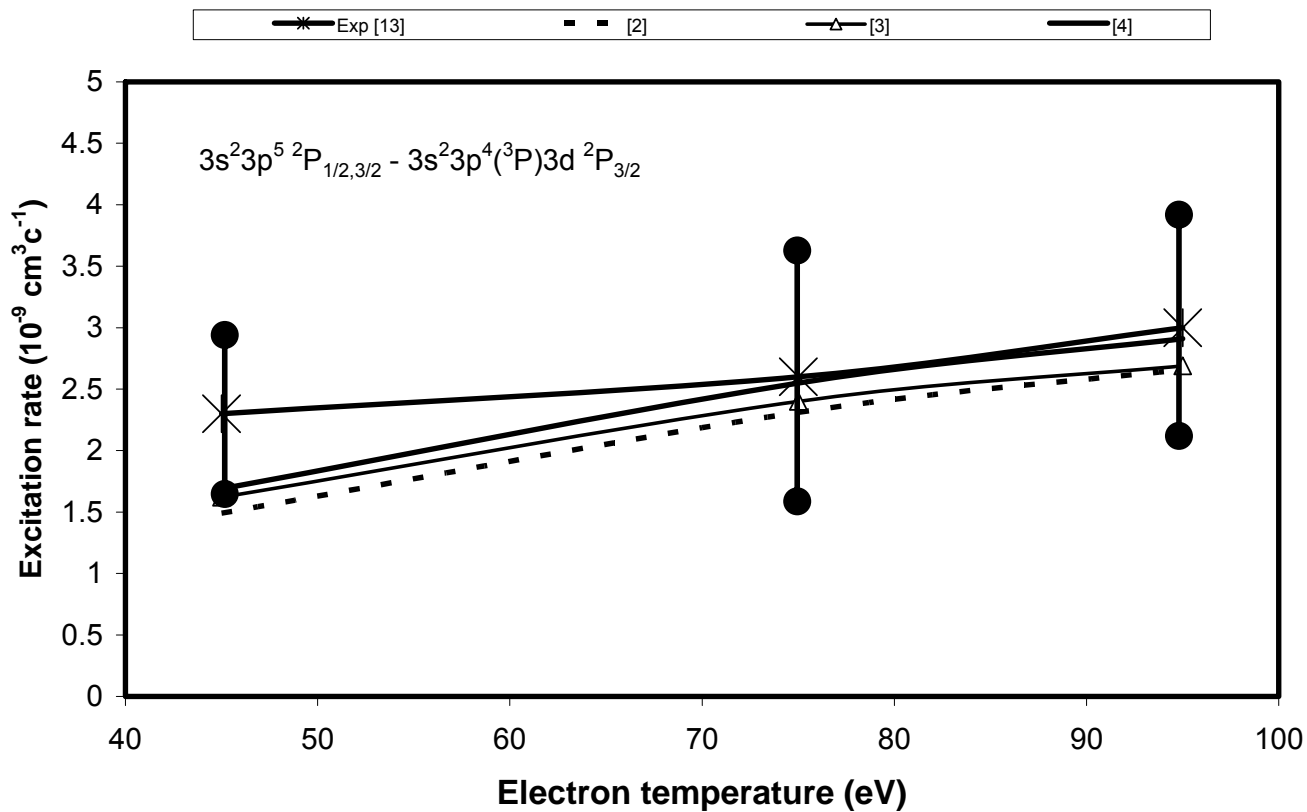


Figure 13. Comparison of experimental and theoretical excitation rates for transition $3s^2 3p^5 \ ^2P_{1/2,3/2} - 3s^2 3p^4 (^3P) 3d \ ^2P_{3/2}$ of Fe X: solid line – [4], dotted line – [2], solid line with * - experiment [13].

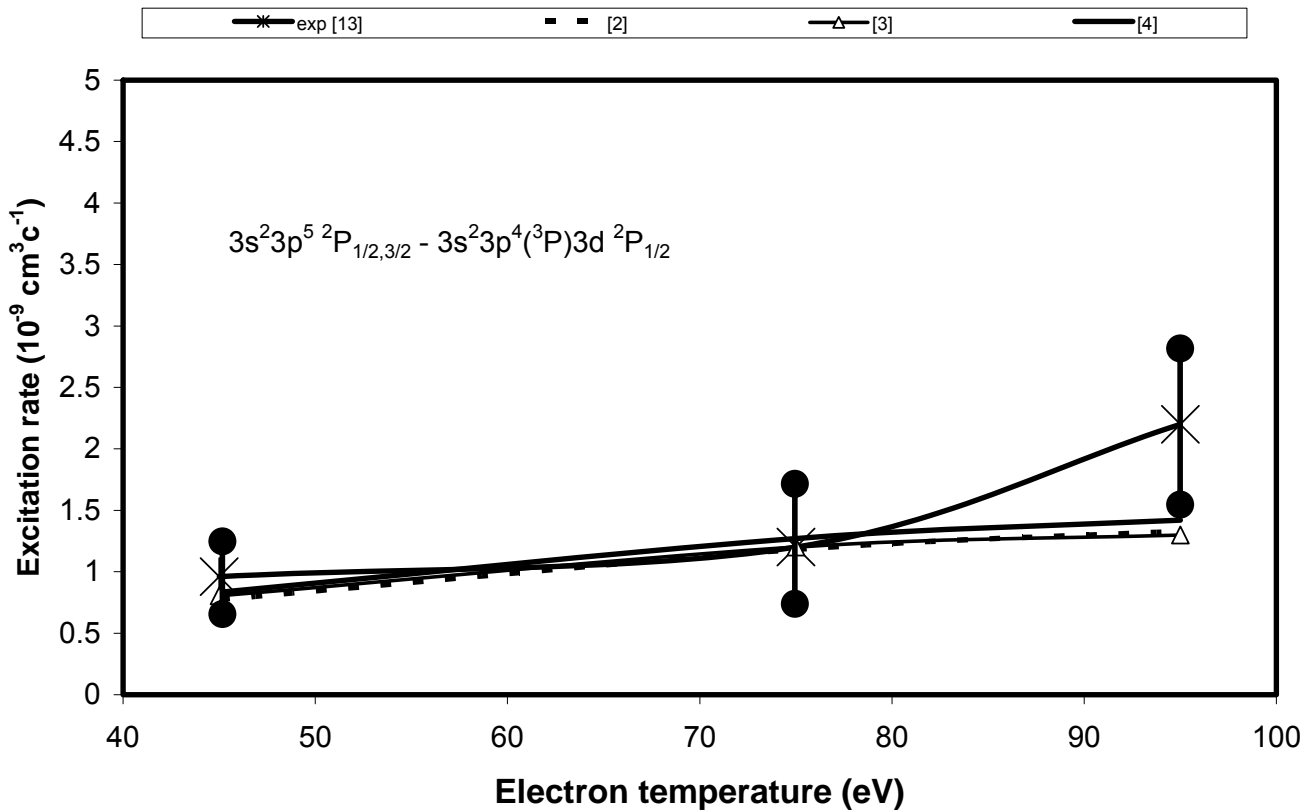


Figure 14. Comparison of experimental and theoretical excitation rates for transition $3s^2 3p^5 \ ^2P_{1/2,3/2} - 3s^2 3p^4 (^3P) 3d \ ^2P_{1/2}$ of Fe X: solid line – [4], dotted line – [2], solid line with * - experiment [13].

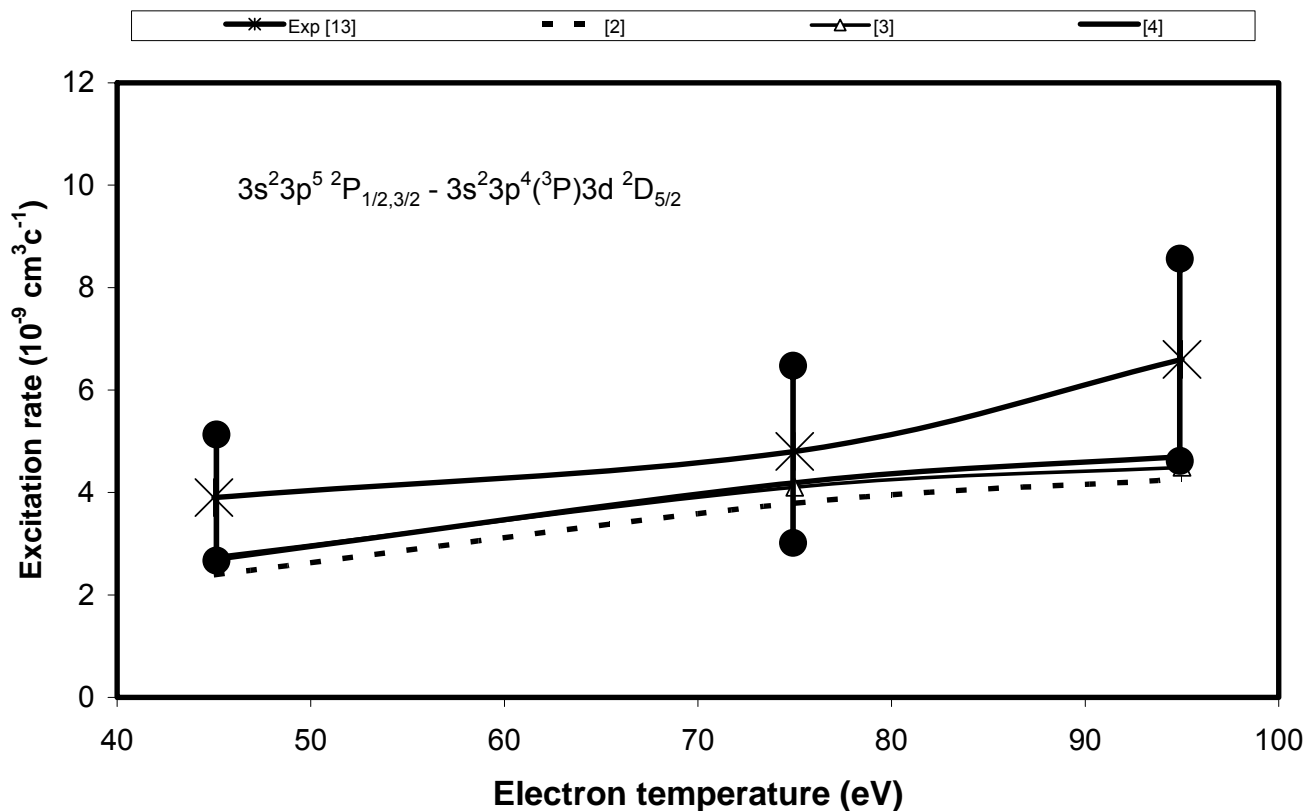


Figure 15. Comparison of experimental and theoretical excitation rates for transition $3s^2 3p^5 \ ^2P_{1/2,3/2} - 3s^2 3p^4 (^3P) 3d \ ^2D_{5/2}$ of Fe X: solid line – [4], dotted line – [2], solid line with * - experiment [13].

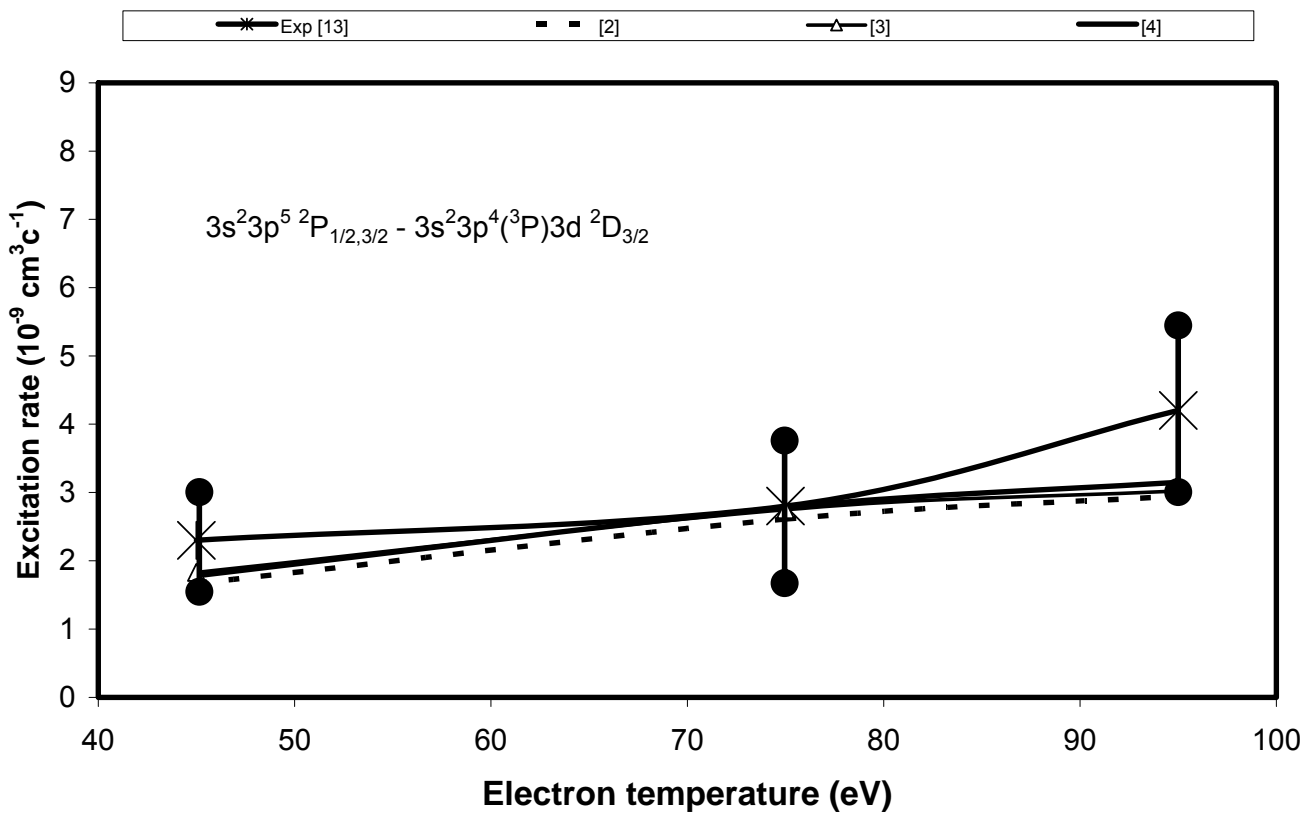


Figure 16. Comparison of experimental and theoretical excitation rates for transition $3s^23p^5\ ^2P_{1/2,3/2} - 3s^23p^4(^3P)3d\ ^2D_{3/2}$ of Fe X: solid line – [4], dotted line – [2], solid line with * - experiment [13].

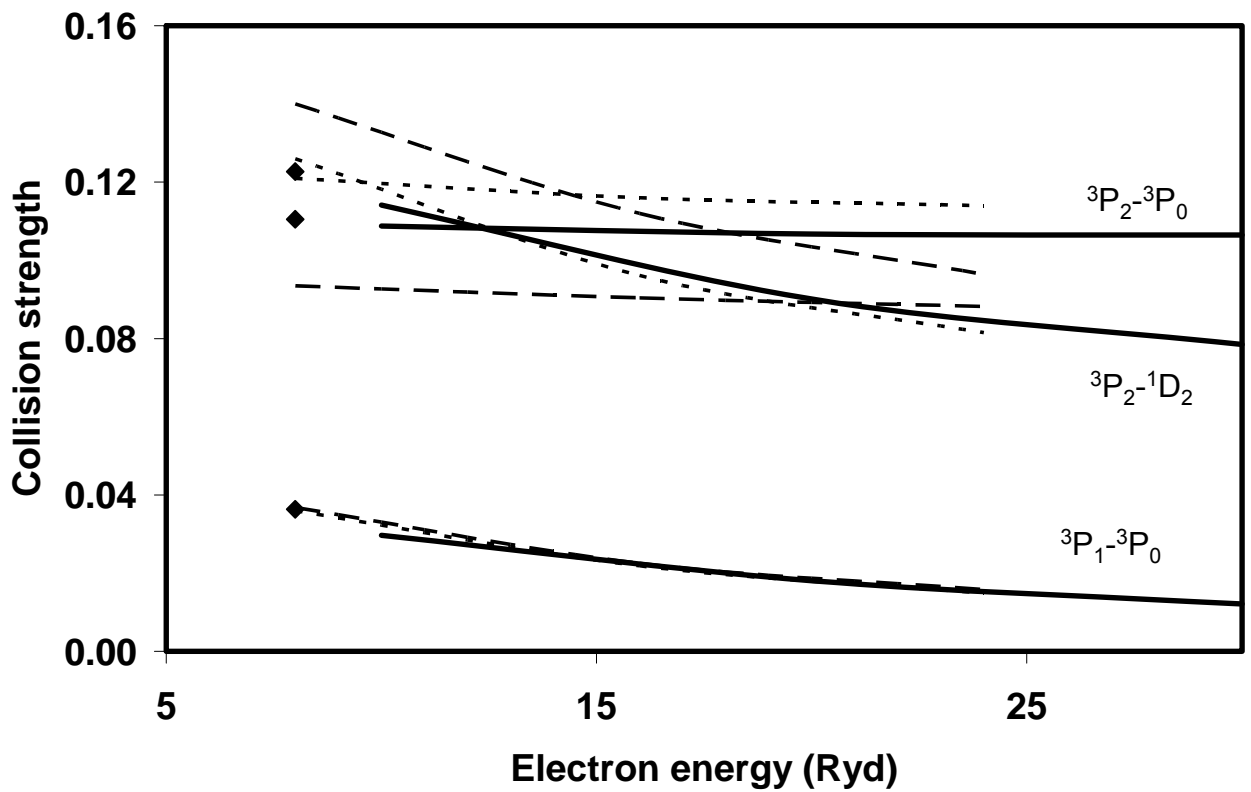


Fig. 17. Comparison of collision strengths, calculated for transitions $3s^23p^4 \ ^3P_J - (2S'+1)L'_J$, of Fe XI: solid lines – [20], dashed lines – [19], dotted lines - [16], \blacklozenge - [17].

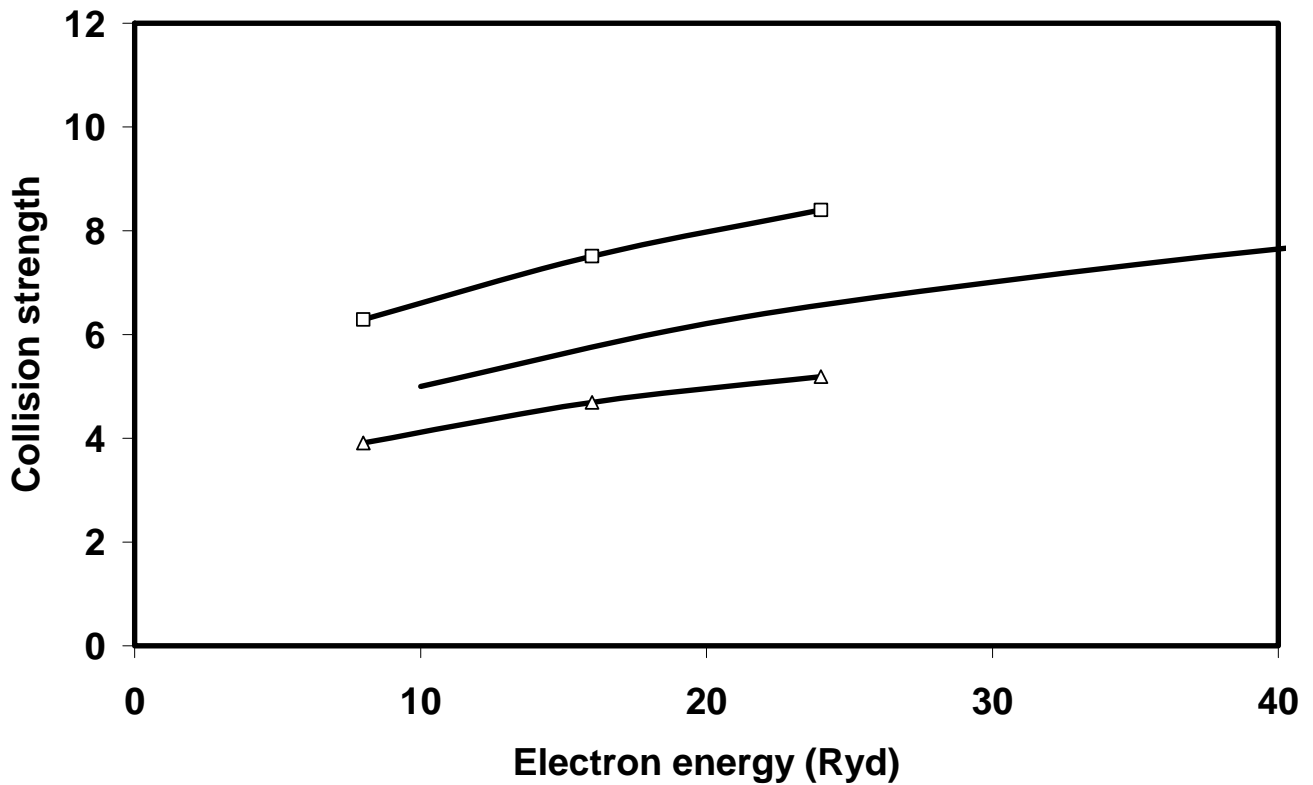


Fig. 18. Comparison of collision strengths, calculated for transition $3s^23p^4 \ ^3P_2 - 3s^23p^3(2D)3d \ ^3P_2$ of Fe XI: solid line without markers – [20], solid line with \square – [16], solid line with \triangle - [19].

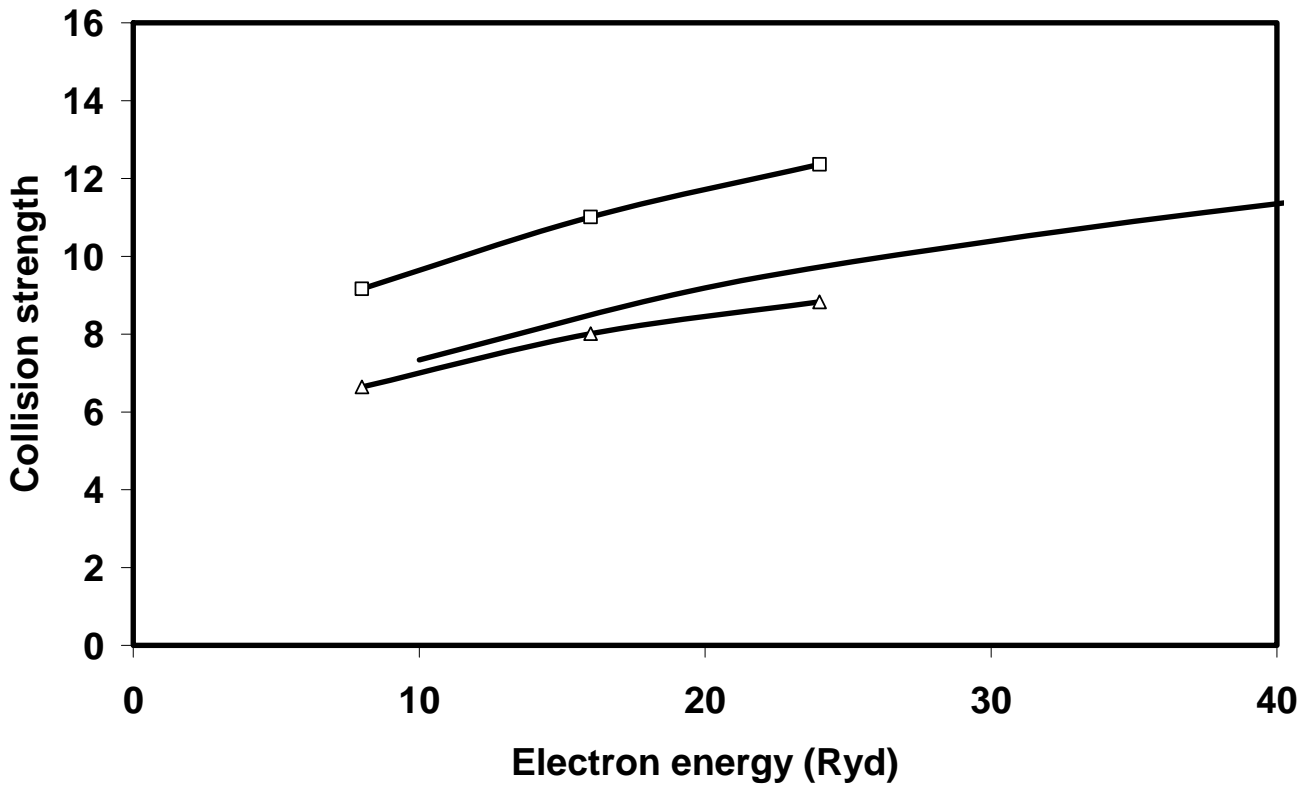


Fig. 19. Comparison of collision strengths, calculated for transition $3s^2 3p^4 \ ^3P_2 - 3s^2 3p^3 (^4S) 3d \ ^3D_3$ of Fe XI: solid line without markers – [20], solid line with \square – [16], solid line with Δ - [19].

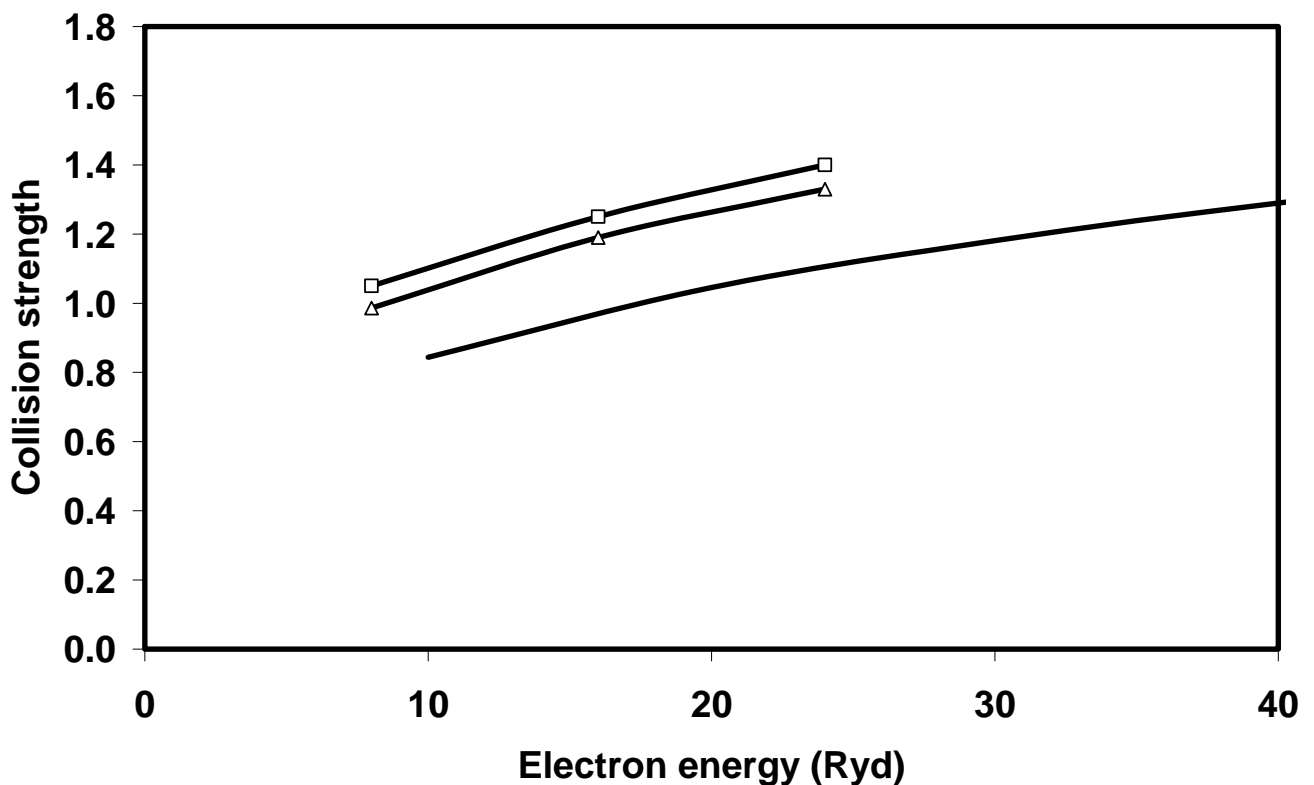


Fig. 20. Comparison of collision strengths, calculated for transition $3s^2 3p^4 \ ^3P_2 - 3s^2 3p^3 (^4S) 3d \ ^3D_2$ of Fe XI: solid line without markers – [20], solid line with \square – [16], solid line with Δ - [19].

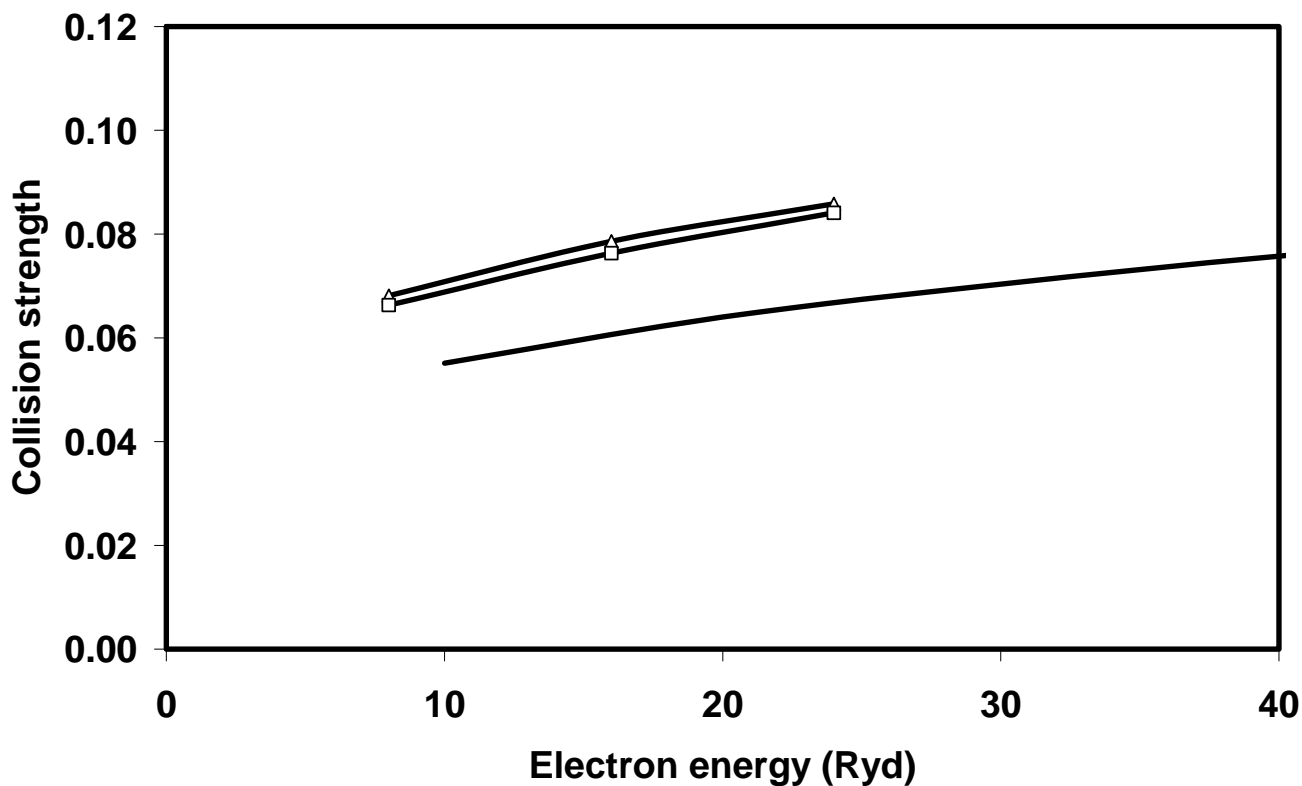


Fig. 21. Comparison of collision strengths, calculated for transition $3s^2 3p^4 \ ^3P_2 - 3s^2 3p^3(^4S) 3d \ ^3D_1$ of Fe XI: solid line without markers – [20], solid line with \square – [16], solid line with \triangle - [19].

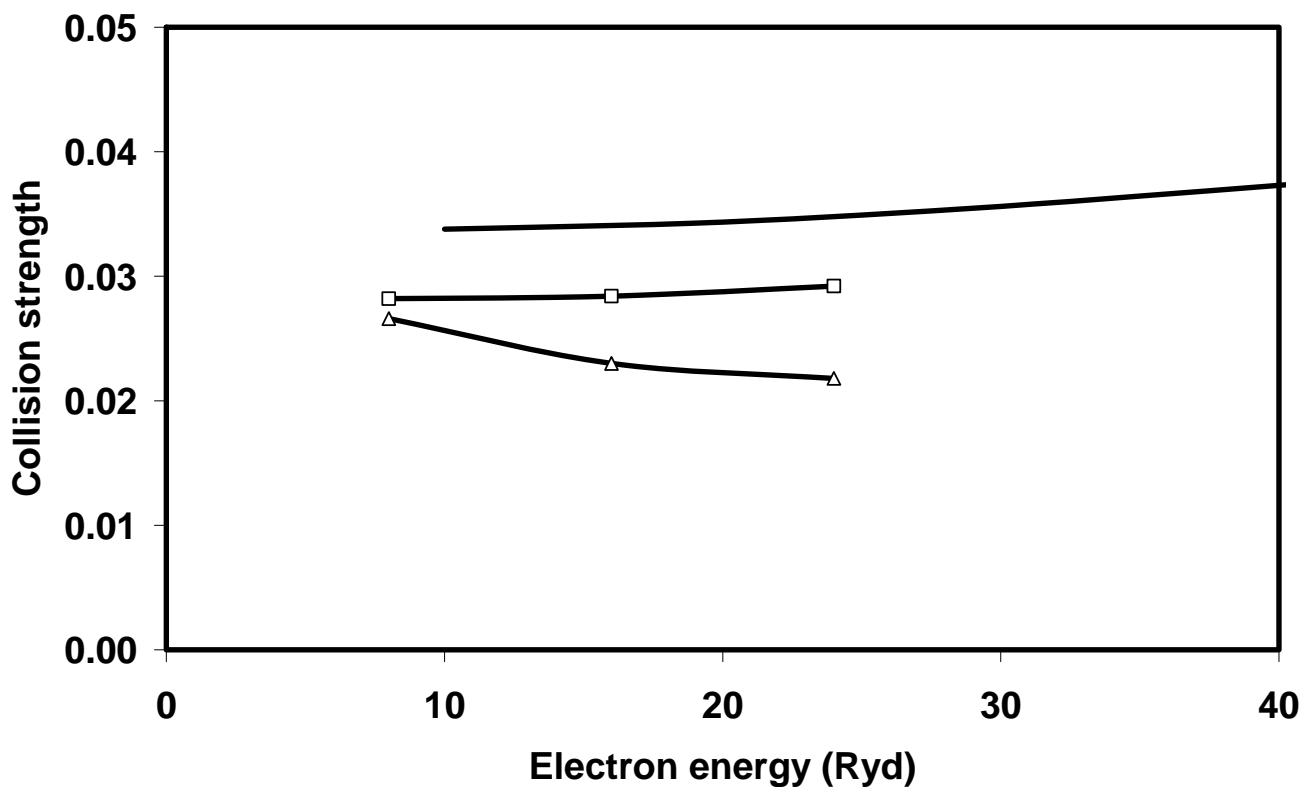


Fig. 22. Comparison of collision strengths, calculated for transition $3s^2 3p^4 \ ^3P_2 - 3s^2 3p^3(^2D) 3d \ ^1D_2$ of Fe XI: solid line without markers – [20], solid line with \square – [16], solid line with \triangle - [19].

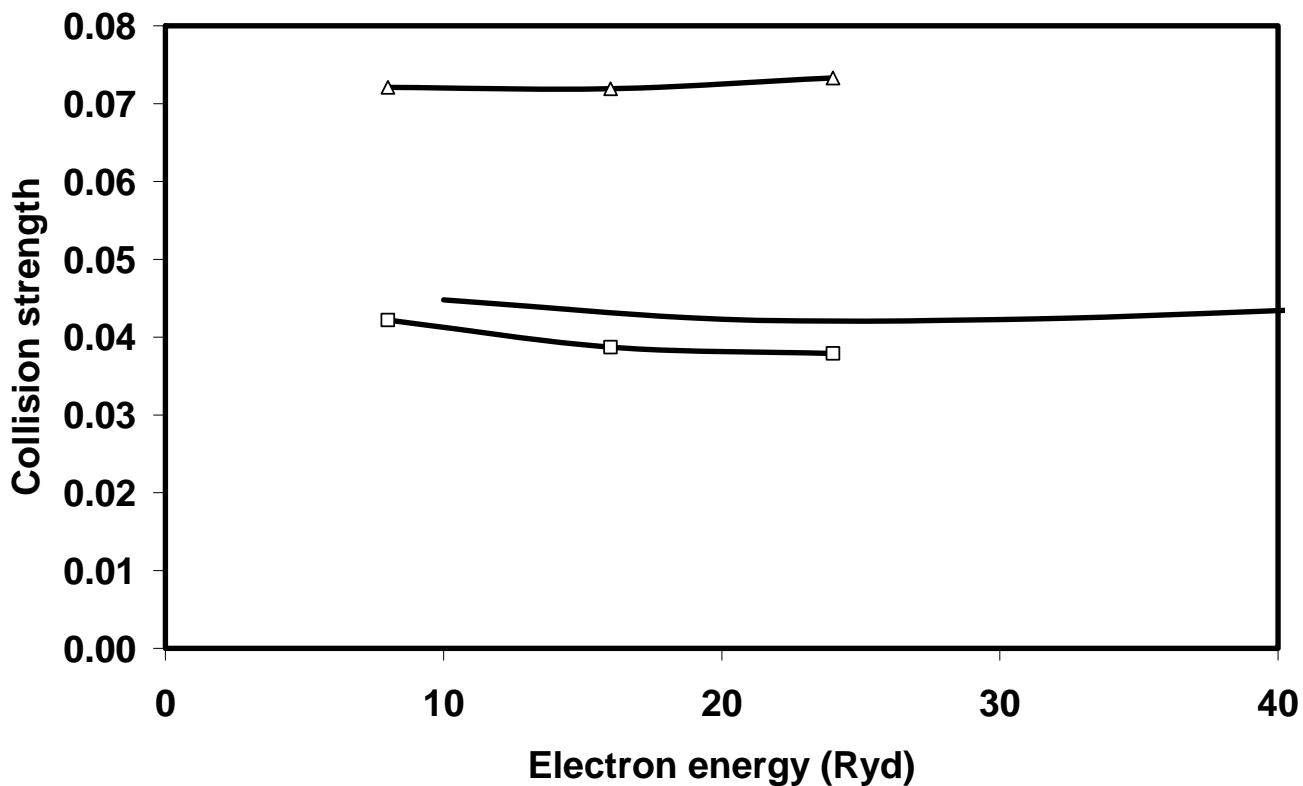


Fig. 23. Comparison of collision strengths, calculated for transition $3s^2 3p^4 \ ^3P_2 - 3s^2 3p^3(^2D)3d \ ^1F_3$ of Fe XI: solid lines without markers – [20], solid lines with \square – [16], solid lines with Δ – [19].

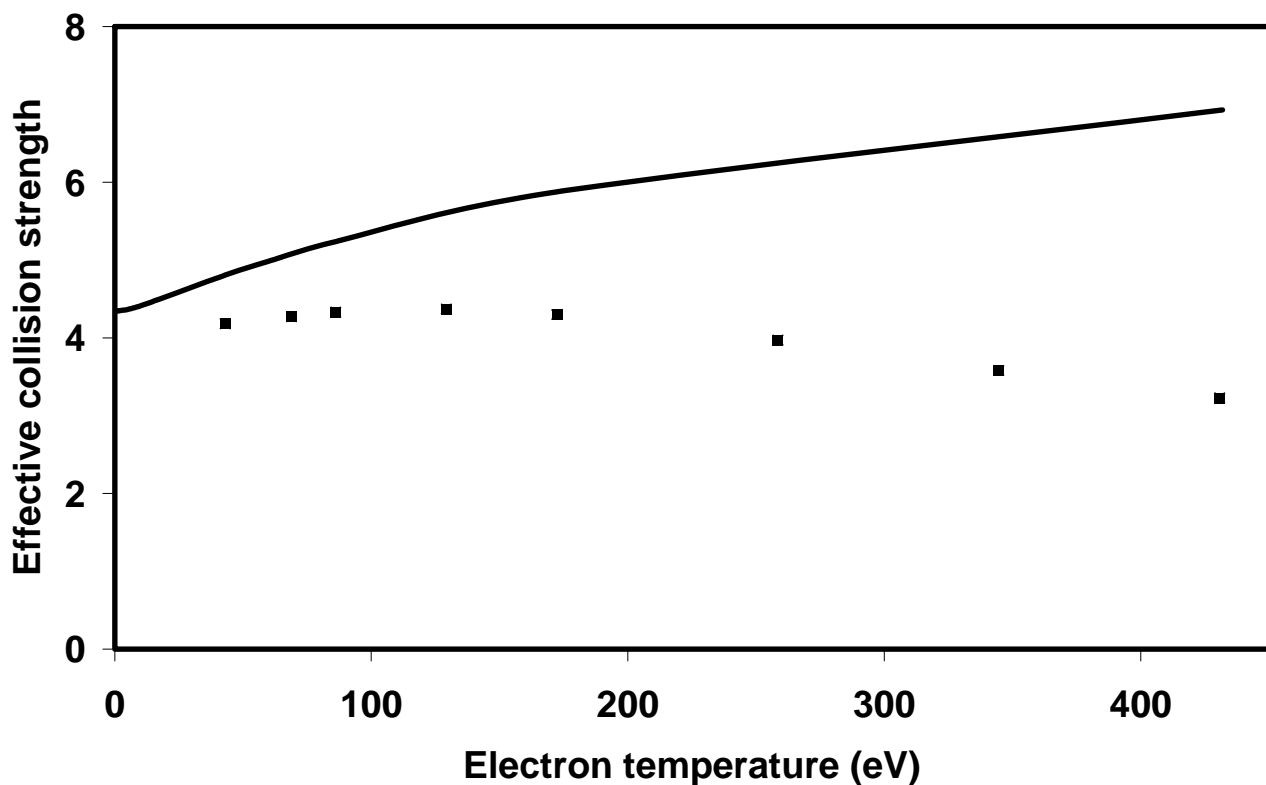


Fig. 24. Comparison of effective collision strengths, calculated for transition $3s^2 3p^4 \ ^3P_2 - 3s^2 3p^3(^2D)3d \ ^3P_2$ of Fe XI: solid line – [21], \blacksquare – [19].

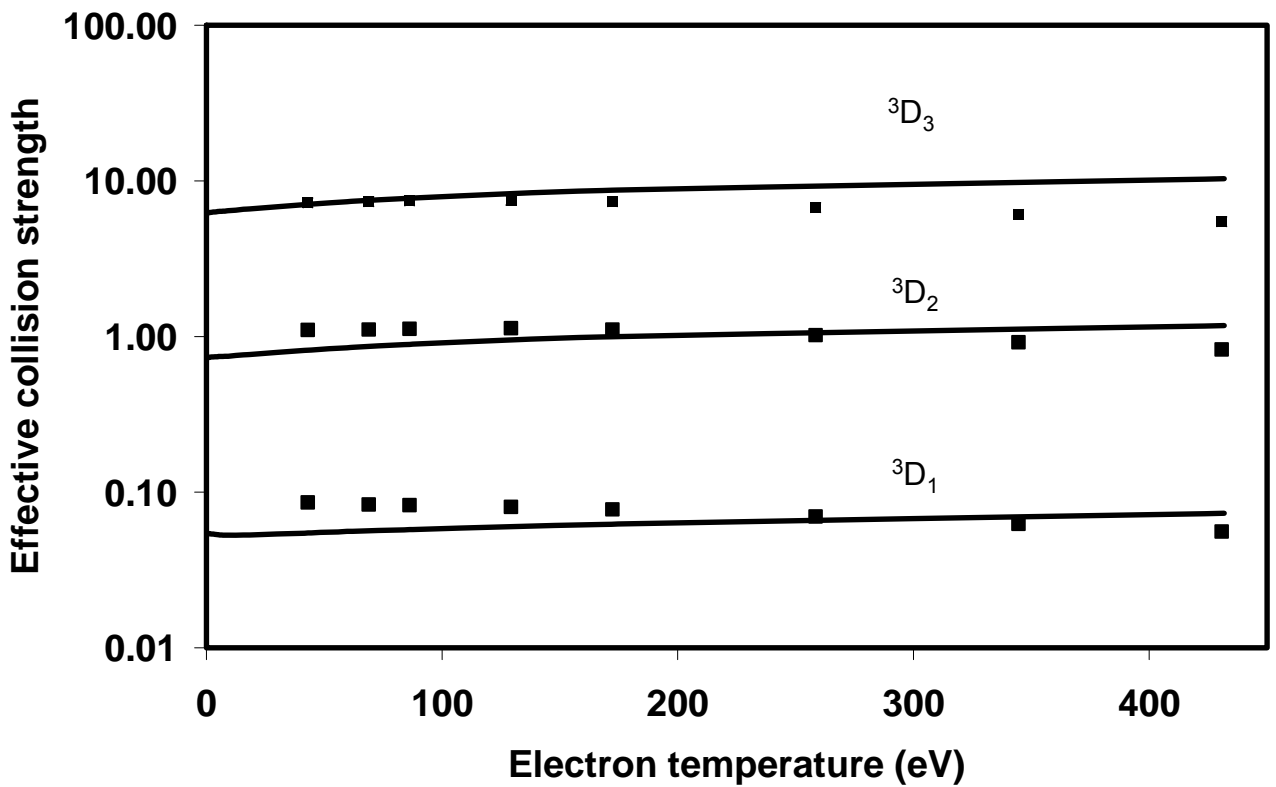


Fig. 25. Comparison of effective collision strengths, calculated for transitions $3s^2 3p^3(4S) 3d\ ^3D_j - 3s^2 3p^3(4S) 3d\ ^3D_j$ of Fe XI: solid lines – [21], ■ – [19].

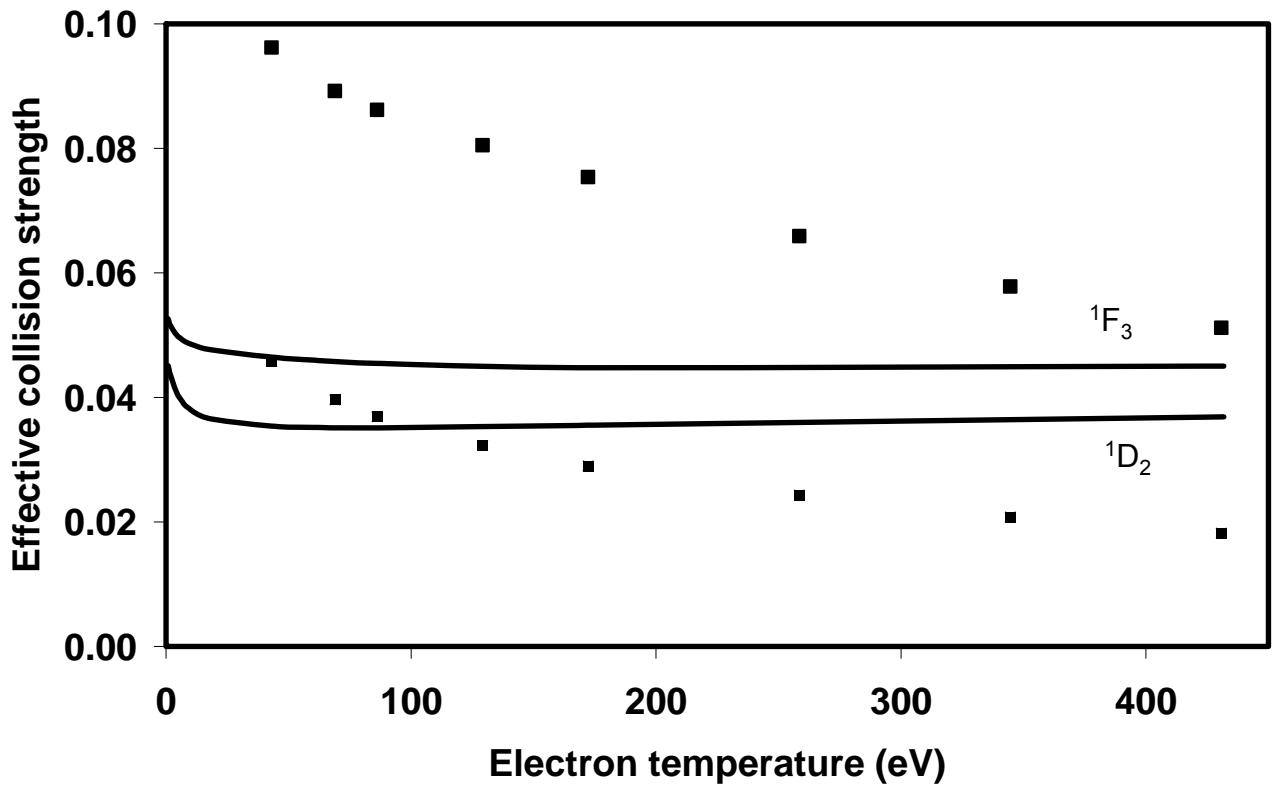


Fig. 26. Comparison of effective collision strengths, calculated for transitions $3s^2 3p^3(2D) 3d\ ^1F_3 - 3s^2 3p^3(2D) 3d\ ^1F_3$ and $^1D_2 - 3s^2 3p^3(2D) 3d\ ^1D_2$ of Fe XI: solid lines – [21], ■ – [19].

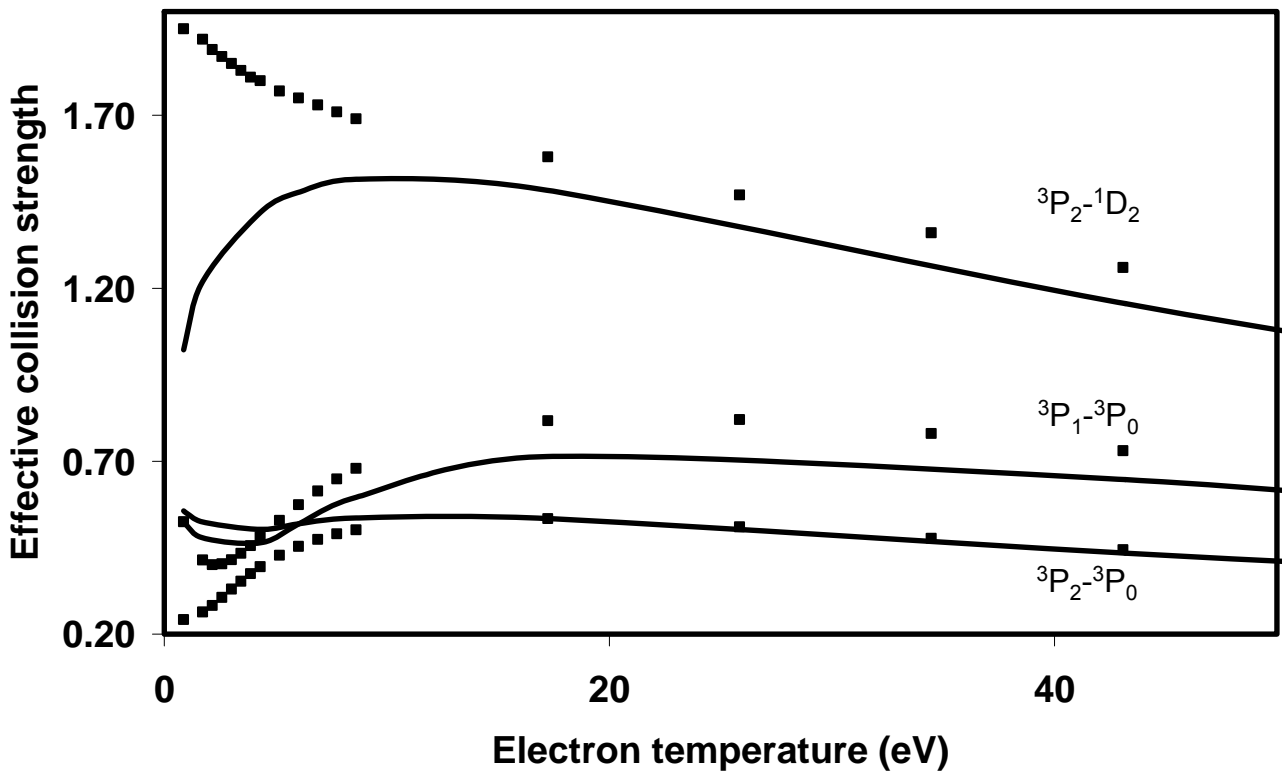


Fig. 27. Comparison of effective collision strengths, calculated for transitions $3s^23p^4 {}^3P_J - 2S^{+1}L'_J$, of Fe XI: solid lines – [21], ■ – [19].

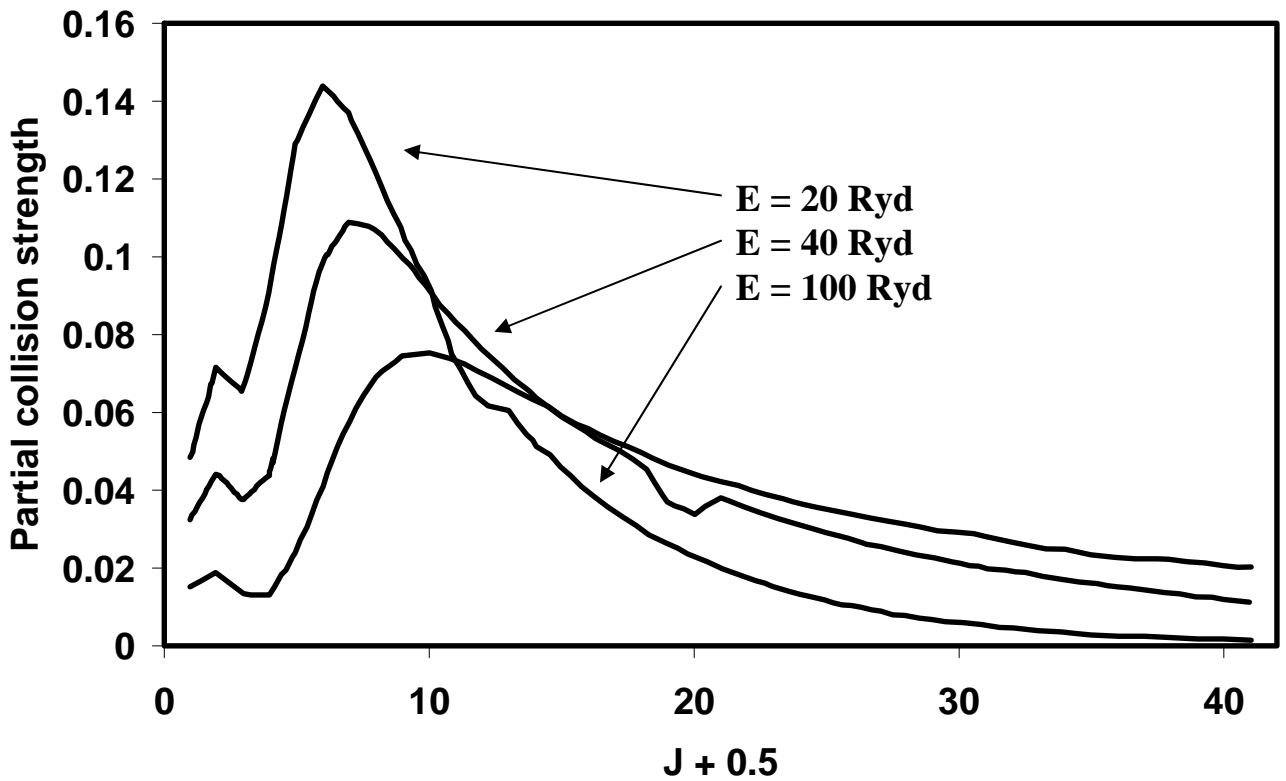


Figure 28. Partial collision strength for $3s^23p^3d {}^1P_1 - 3p^6 {}^1S_1$ transition of Fe XI at different energies.

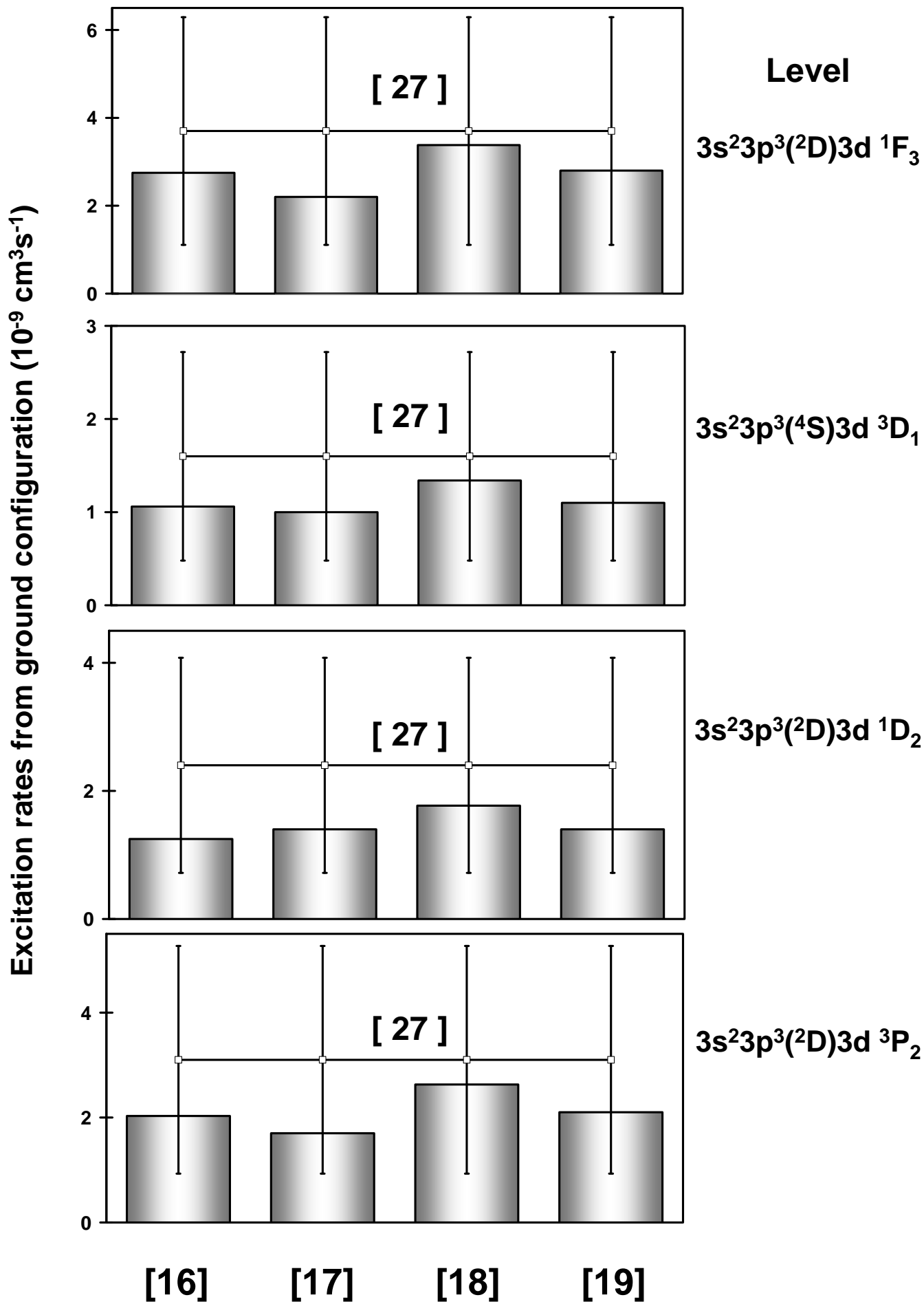


Fig. 29. Comparison of experimental [27] and theoretical [16-19] values of excitation rates for some levels of Fe XI.

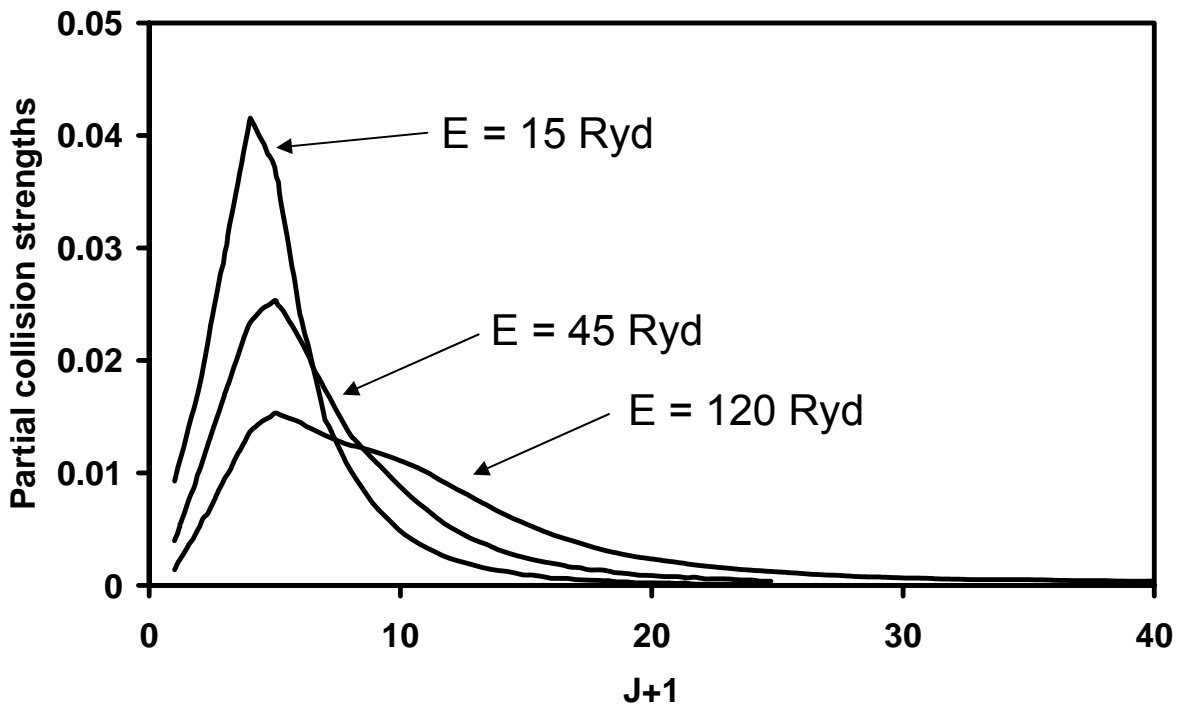


Fig. 30. Partial collision strengths [31] for the $3s^2 3p^2 \ ^3P_1 - 3s^2 3p^2 \ ^3P_2$ transition of Fe XIII at different energies E of electron.

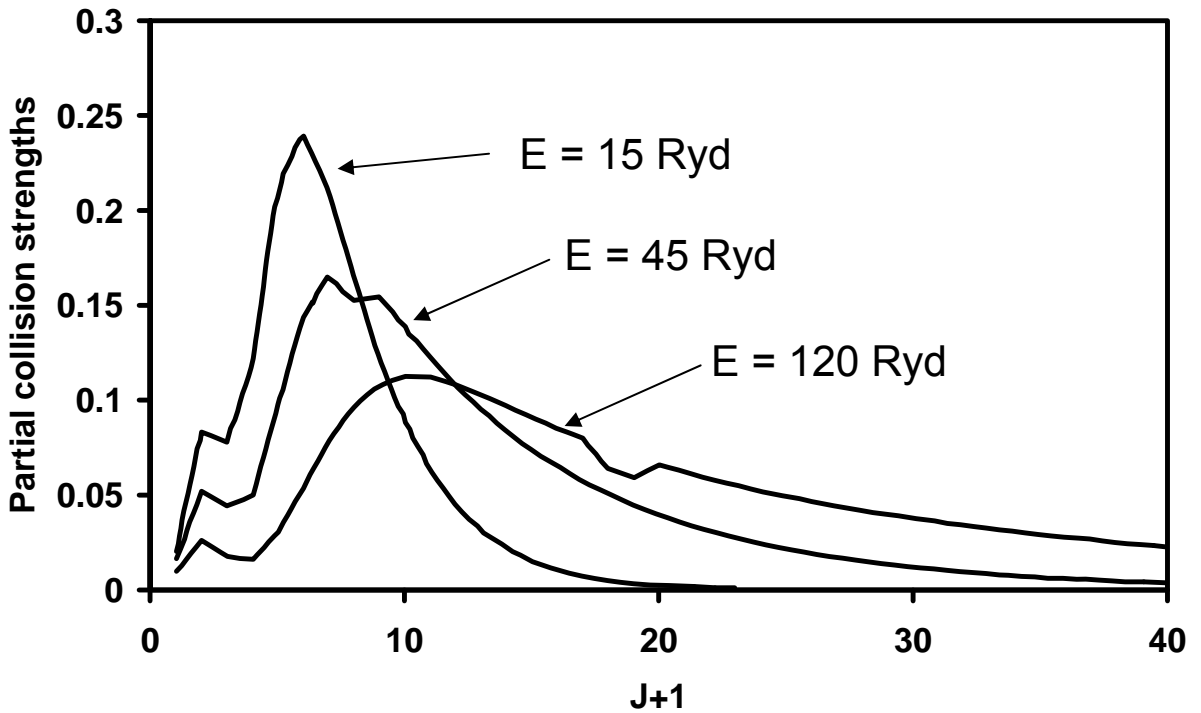


Fig. 31. Partial collision strengths [31] for the $3s^2 3p^2 \ ^3P_1 - 3s^2 3p 3d \ ^3D_1$ transition of Fe XIII at different energies E of electron.

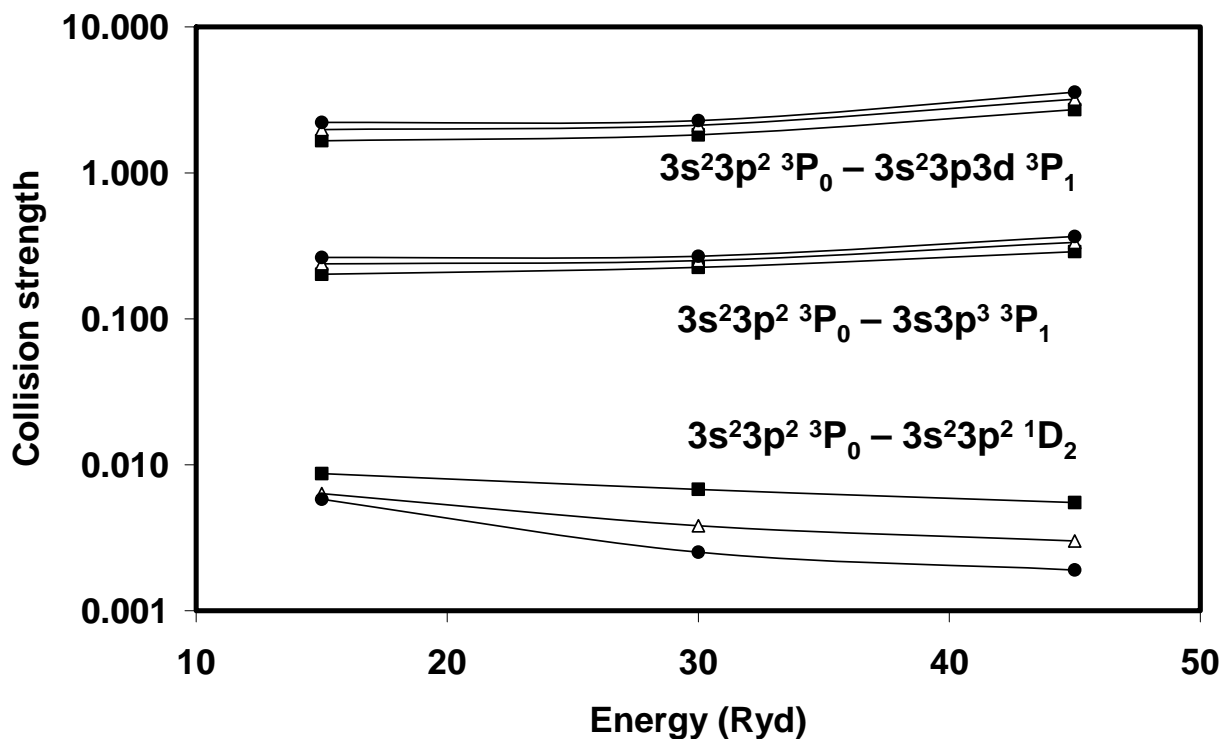


Fig. 32. Collision strengths for some transition of Fe XIII calculated in papers [31] (■), [30] (△) and [28] (●).

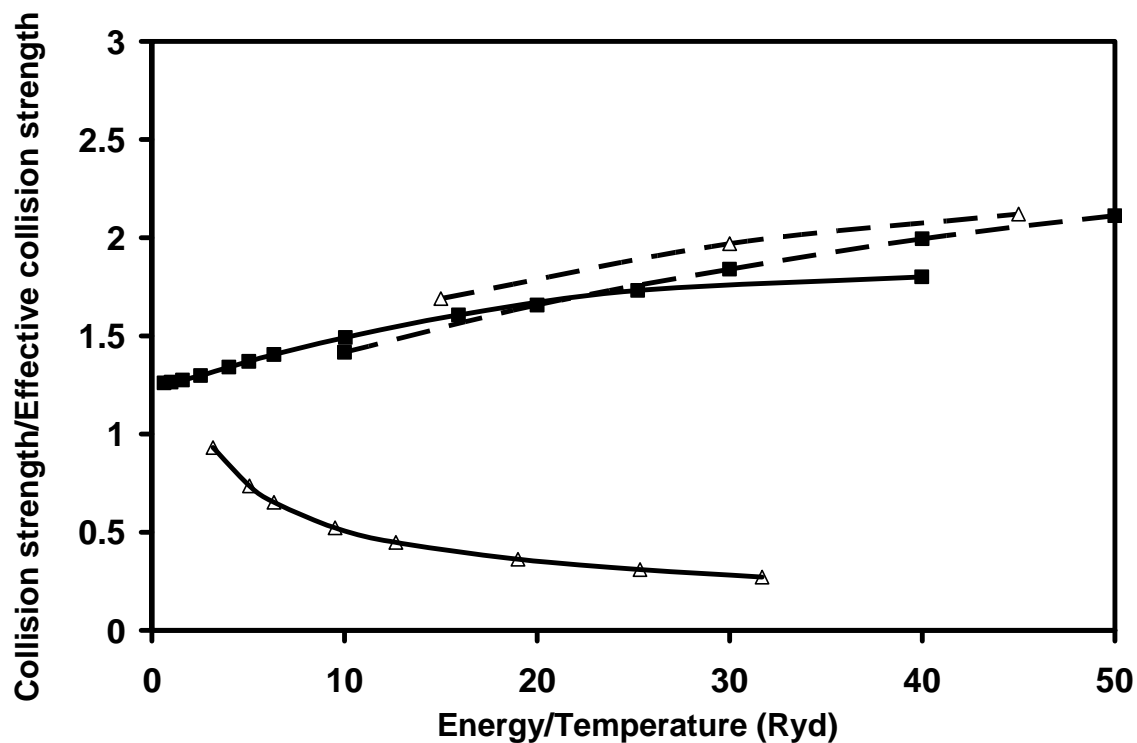


Fig. 33. Collision strengths (dashed lines) and effective collision strength (solid lines) for transition $3s^2 3p^2 \ ^3P_1 - 3s^2 3p 3d \ ^3D_1$ of Fe XIII calculated in papers [31] (■), and [30] (△).

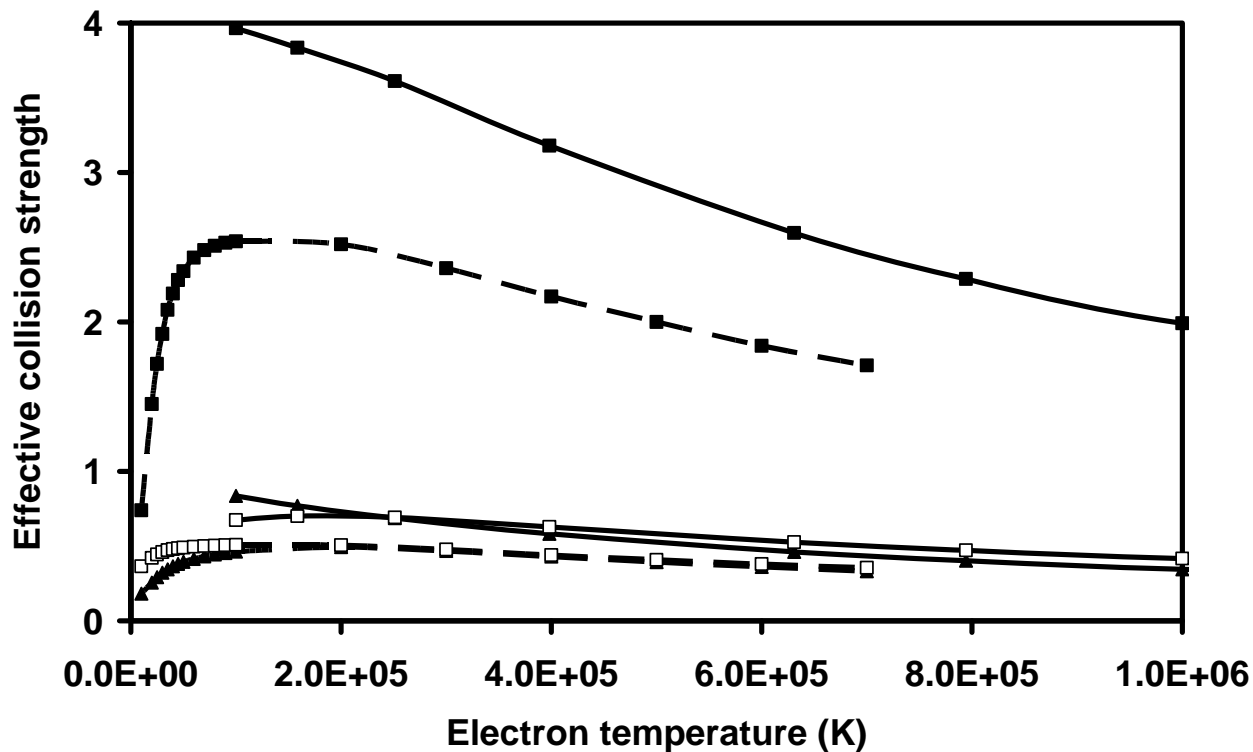


Fig. 34. Effective collision strength for transitions $3s^2 3p^2 \ ^3P_0 - 3s^2 3p^2 \ ^3P_1$ (\blacktriangle), $3s^2 3p^2 \ ^3P_0 - 3s^2 3p^2 \ ^3P_2$ (\square), and $3s^2 3p^2 \ ^3P_1 - 3s^2 3p^2 \ ^3P_2$ (\blacksquare) of Fe XIII calculated in papers [32] (solid lines), and [30] (dashed lines).

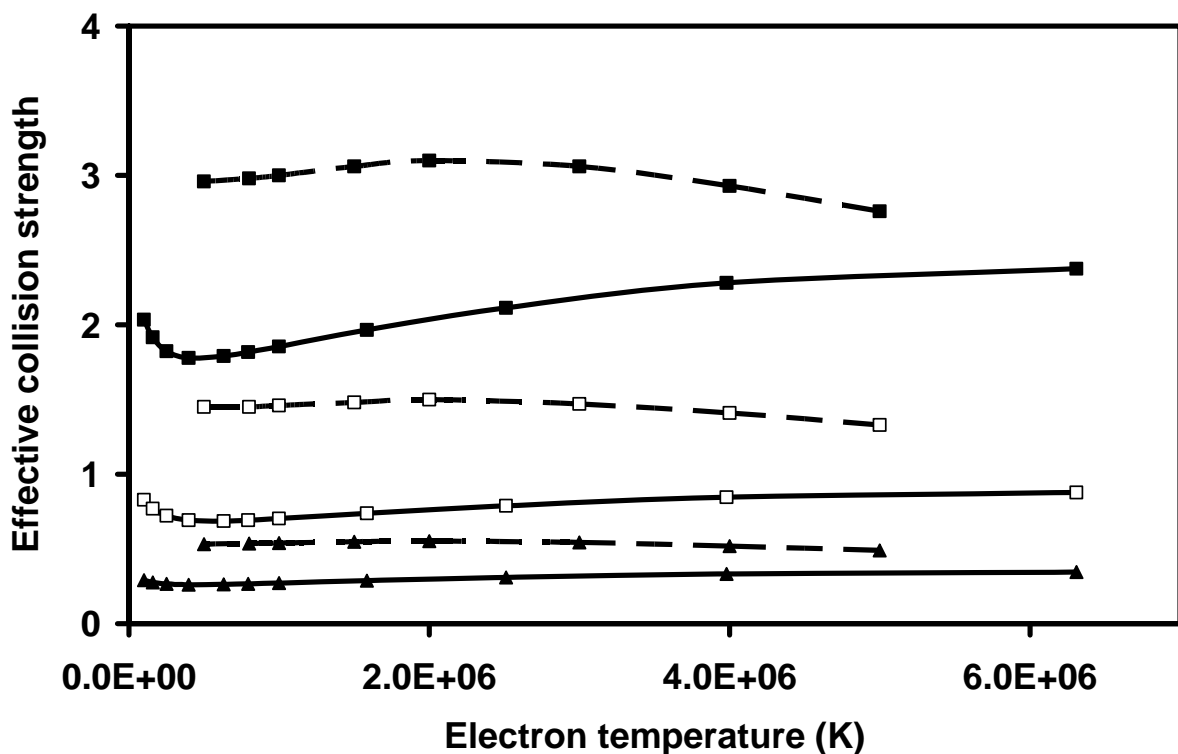


Fig. 35. Effective collision strength for transitions $3s^2 3p^2 \ ^3P_0 - 3s 3p^3 \ ^3S_1$ (\blacktriangle), $3s^2 3p^2 \ ^3P_1 - 3s 3p^3 \ ^3S_1$ (\square), and $3s^2 3p^2 \ ^3P_2 - 3s 3p^3 \ ^3S_1$ (\blacksquare) of Fe XIII calculated in papers [32] (solid lines), and [30] (dashed lines).

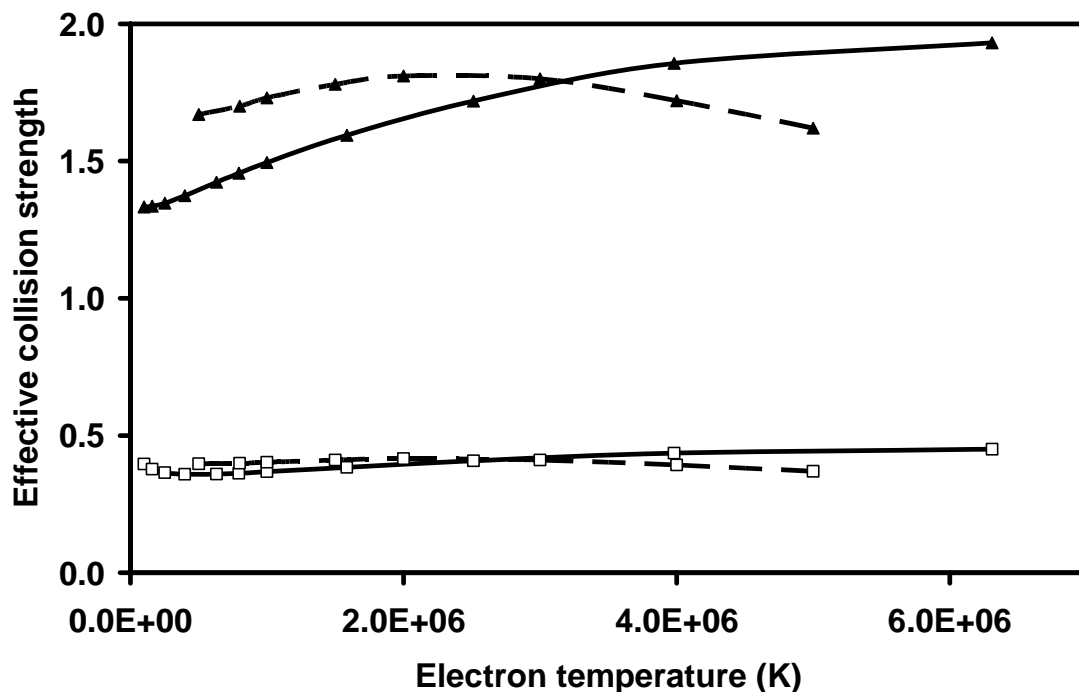


Fig. 36. Effective collision strength for transitions $3s^23p^2\ ^3P_0 - 3s^23p3d\ ^3P_1$ (▲) and $3s^23p^2\ ^3P_2 - 3s^23p3d\ ^3P_1$ (□) of Fe XIII calculated in papers [32] (solid lines) and [30] (dashed lines).

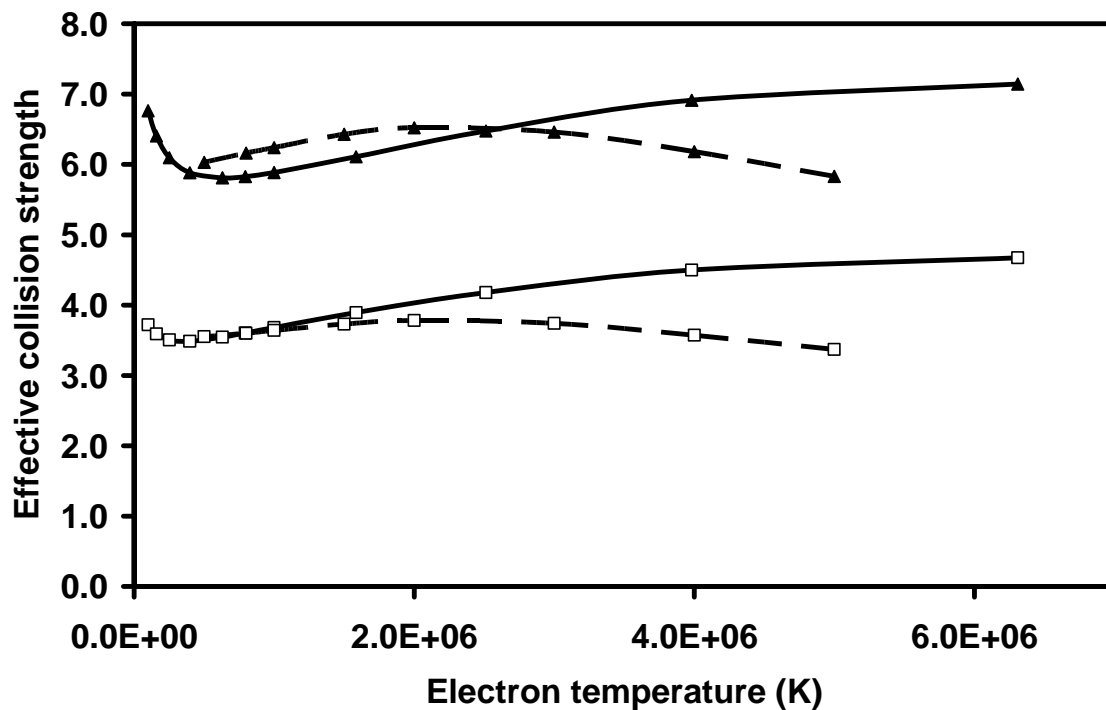


Fig. 37. Effective collision strength for transitions $3s^23p^2\ ^3P_2 - 3s^23p3d\ ^3D_3$ (▲) and $3s^23p^2\ ^1D_2 - 3s^23p3d\ ^1D_2$ (□) of Fe XIII calculated in papers [32] (solid lines) and [30] (dashed lines).